Exciton dynamics in photosynthetic molecular aggregates

by

Johan Antowan Nöthling

Submitted in partial fulfilment of the requirements for the degree

Magister Scientiae

in the Department of Physics
in the Faculty of Natural and Agricultural Sciences
University of Pretoria
Pretoria

April 2016

UNIVERSITEIT VAN PRETORIA
UNIVERSITY OF PRETORIA
YUNIBESITHI YA PRETORIA

Abstract

Exciton dynamics in photosynthetic molecular aggregates

by

Johan Antowan Nöthling

Supervisor:	Dr. T.P.J. Krüger
Co-supervisor:	Prof. T. Mančal
Degree:	*Magister Scientiae*
Keywords:	Exciton dynamics, Redfield theory, Photosynthesis, Light-harvesting

Almost all of the energy that sustains life on Earth was captured from sunlight during the process of photosynthesis. In the first step of this process, photons are absorbed by aggregates of pigment molecules called light-harvesting complexes. In these complexes, pigment molecules are carefully arranged by protein backbones and are consequently able to absorb excitation at much higher pigment concentration than for the same pigments in solution. The close proximity of pigment molecules in light-harvesting complexes may cause significant interaction between them and consequent delocalisation of excitation over more than one pigment molecule. These delocalised states are called *exciton* states. The electronic degrees of freedom of pigment molecules are modulated by the large number of vibrational modes in the protein backbone and pigments themselves. In many light-harvesting complexes, the interaction between pigment molecules are much stronger than interaction with the vibrational modes. In such systems, a formalism called Redfield theory, which treats interaction with vibrations perturbatively, can be used to calculate exciton dynamics.

In this dissertation, we give an overview of the process of photosynthesis and the

UNIVERSITEIT VAN PRETORIA
UNIVERSITY OF PRETORIA
YUNIBESITHI YA PRETORIA

physical mechanisms underlying light-harvesting. We then derive the Redfield equation and explain its use in systems containing a single or multiple excitations. We illustrate calculation of Redfield-dynamics by computing the exciton dynamics in three systems: a six-member ring demonstrating essential features of exciton dynamics; FMO, a conduit for excitation in green sulphur bacteria and LHCII, the main light-harvesting complex in green plants.

UNIVERSITEIT VAN PRETORIA
UNIVERSITY OF PRETORIA
YUNIBESITHI YA PRETORIA

Samevatting

Eksitondinamika in fotosintetiese molekulêre aggregate

deur

Johan Antowan Nöthling

Studieleier:	Dr. T.P.J. Krüger
Medestudieleier:	Prof. T. Mančal
Graad:	*Magister Scientiae*
Sleutelwoorde:	Eksitondinamika, Redfieldteorie, Fotosintese, Ligversameling

Bykans al die energie wat lewe op Aarde onderhou is vanuit sonligenergie vasgevang tydens die proses van fotosintese. In die eerste stap van hierdie proses word fotone deur aggregate van pigmentmolekules, wat ligversamelingskomplekse genoem word, geabsorbeer. In hierdie komplekse verleen ’n proteïenraamwerk presiese rangskikking aan die pigmentmolekules, wat gevolglik energie by veel hoër pigmentkonsentrasie as in oplossing kan absorbeer. Die klein afstande tussen pigmentmolekules in ligversamlingskomplekse kan sterk interaksie tussen hierdie molekules teweegbring en daarom tot delokalisering van opwekking oor meer as een pigmentmolekuul lei. Sulke gedelokaliseerde toestande word eksitontoestande genoem. Die pigmentmolekules se elektroniese vryheidsgrade word deur die groot hoeveelheid vibrasies in die proteïenstruktuur, en in pigmentmolekules self, beïnvloed. In baie ligversamelingskomplekse is die interaksie tussen pigmentmolekules veel sterker as die interaksie met vibrasies. In sulke gevalle gee ’n teoretiese raamwerk, genaamd Redfieldteorie, wat interaksie met vibrasies as ’n perturbasie hanteer, ’n akkurate beskrywing van eksitondinamika.

In hierdie verhandeling gee ons ’n oorsig van fotosintese en die fisiese megan-

UNIVERSITEIT VAN PRETORIA
UNIVERSITY OF PRETORIA
YUNIBESITHI YA PRETORIA

ismes wat dit onderlê. Ons lei dan die Redfieldvergelyking af en verduidelik hoe dit gebruik kan word om die dinamika van enkeleksiton- of veeleksitonstelsels te bereken. Ons illustreer die berekening van Redfielddinamika in drie voorbeeldstelsels: 'n seslid ring wat belangrike eienskappe in sy dinamika toon; FMO, 'n energiegeleier in groenswaelbakterieë en LHCII, die hoof ligversamelingskompleks van groen plante.

Declaration

I, Johan Antowan Nöthling declare that the dissertation, which I hereby submit for the degree *Magister Scientiae* at the University of Pretoria, is my own work and has not previously been submitted by me for a degree at this or any other tertiary institution.

Signature:	.....
	Johan Antowan Nöthling
Student number:	1057 1460
Date:	15th April 2016

UNIVERSITEIT VAN PRETORIA
UNIVERSITY OF PRETORIA
YUNIBESITHI YA PRETORIA

Acknowledgements

- My supervisor Dr. T.P.J. Krüger for his guidance, encouragement and empathy.
- My co-supervisor Prof. T. Mančal for his interest, assistance and immense patience.
- My family and friends for their love, support and encouragement.
- Louwrens van Schalkwyk for the LaTeX template from which this document was compiled.
- The Almighty God for giving us enough questions to ponder and just enough answers to keep us interested.

Financial Support

Financial support provided by the National Institute for Theoretical Physics (NITheP)[1] in respect of the costs of the study is hereby acknowledged.

[1]Disclaimer: Any opinion, findings and conclusions or recommendations in this material are those of the author(s) and therefore NITheP do not accept any liability in regard thereto.

UNIVERSITEIT VAN PRETORIA
UNIVERSITY OF PRETORIA
YUNIBESITHI YA PRETORIA

Dedications

For my parents.

Dankie!

UNIVERSITEIT VAN PRETORIA
UNIVERSITY OF PRETORIA
YUNIBESITHI YA PRETORIA

"When life gives you lemons...How heavy are they? What happens when we let two collide? At what rate do they decay? Can we make lemonade that tastes like coffee?"

- A physicist

UNIVERSITEIT VAN PRETORIA
UNIVERSITY OF PRETORIA
YUNIBESITHI YA PRETORIA

Contents

UNIVERSITEIT VAN PRETORIA
UNIVERSITY OF PRETORIA
YUNIBESITHI YA PRETORIA

UNIVERSITEIT VAN PRETORIA
UNIVERSITY OF PRETORIA
YUNIBESITHI YA PRETORIA

Chapter 1

Introduction

1.1 Photosynthesis: the indispensable process

The very existence of life on earth is astonishing! Living organisms are immensely complex and ordered systems. Bringing about, and maintaining this complex order requires a very large amount of energy. Almost all of the energy stored in living organisms, the chemical compounds they produce and their decomposed forms reached the earth as electromagnetic radiation from the sun. This energy was absorbed into the biosphere by photosynthesis, a process in which light energy is captured by living organisms and converted to storable chemical energy.

To get an idea of the scale of photosynthesis, one should consider the global outputs of the process. Through photosynthesis, energy is stored at an average rate of 130 TW [1]; about ten times as fast as the total human population consumes energy [2]. Organic matter is produced at 1.5×10^{14} kg per year [3]; about three hundred times the collective mass of all humans on earth [4]. And molecular oxygen is produced at 4×10^{14} kg per year [5]; enough to supply the total human population for about 190 years [6].

UNIVERSITEIT VAN PRETORIA
UNIVERSITY OF PRETORIA
YUNIBESITHI YA PRETORIA

Photosynthesis provides energy to a range of terrestrial and aquatic ecosystems. On land, plants are the main primary producers (organisms that produce biomass from inorganic compounds) [7]. During the process of photosynthesis, plants produce high-energy biologically usable compounds from CO_2. This is known as CO_2-fixation. Some of the energy that was stored by plants during photosynthesis is passed through the food network to heterotrophs, thereby sustaining virtually all land animals and many other organisms: the bacteria, protozoa and fungi in the stomachs of ruminants [8], yeast used to ferment beer [9] and archaea decomposing organic matter in rice fields [10]. Almost all other terrestrial organisms also depend on photosynthesis; either being photosynthetic primary producers themselves or using the energy harvested by photosynthesisers (like the fungi in lichen that are in a symbiotic relationship with algae or cyanobacteria [11]).

About half of the global CO_2-fixation happens in the ocean, mainly by cyanobacteria [12]. It is due to the oxygenic photosynthesis by these bacteria that the earth's atmosphere is saturated with oxygen today [13]. Many other organisms in the oceans are photosynthetic: from ordinary kelp [14] to the incredibly patterned diatoms [15].

Not all life depend on the sun for energy, though. In the ocean, sunlight reaches only a certain depth, and virtually all photosynthesis is restricted to this "photic layer" [16]. Near hydrothermal vents, thriving ecosystems of chemoautotrophic microbes and eukaryotes feeding on them, obtain their energy from the released heat and energy-rich inorganic chemical compounds released by the vents [17]. A green sulphur bacterium has even been isolated that uses the faint glow emitted by some hydrothermal vents to photosynthesise [18]. Sunlight-independent organisms are not limited to the deep ocean, but also exist deep under earth's surface: a chemoautotrophic bacteria was found in South-African gold mines 2.8 km beneath the surface [19]!

UNIVERSITEIT VAN PRETORIA
UNIVERSITY OF PRETORIA
YUNIBESITHI YA PRETORIA

It is remarkable that photosynthesis-independent life forms exist only in such isolated places and on such small scales. It seems as though photosynthesis was not merely a lucky participant in an evolutionary race, but by far the *best* energy-delivering mechanism. Photosynthesis has three apparently unique attributes: it provides enough energy to account for the global energy needs of life, it is sufficiently dispersed to maintain similar ecosystems over large distances (because of the uniformity of sunlight), and energy is harvested on the molecular level during photosynthesis (thereby making microbial photoautotrophy possible).

Most other energy-delivering mechanisms that one could devise fall short on one of the above features. Typical temperature gradients on earth are too diffuse for thermal energy to be harvestable at all, nuclear decay processes are spatially very isolated, wind and tide energy provides too little total energy and is also not harvestable on the molecular level. Perhaps photosynthesis really is the **only** process able to maintain life as we know it...

It is clear that photosynthesis is an extremely important process! This is reason enough to study it. In addition, there is a hope that the design principles existing in photosynthesis can be applied to artificial systems in the drive towards cleaner, cheaper and more efficient alternative energy sources [20–23]. Furthermore, if the efficiency of natural photosynthesis can be improved, crop yield could be increased [24–26]. The study of photosynthesis therefore also has commercial incentive.

1.2 Overview of photosynthesis in plants

This section (1.2) is based on the description of photosynthesis in Campbell and Reece (2008) [3], except where another citation is given.

UNIVERSITEIT VAN PRETORIA
UNIVERSITY OF PRETORIA
YUNIBESITHI YA PRETORIA

During photosynthesis, energy from electromagnetic radiation is converted into chemical energy. In plants, the process of photosynthesis essentially consists of a light-dependent phase and light-independent phase. Although the latter is not directly dependent on light intensity, it does depend on the compounds produced during the light-dependent phase.

In this thesis, we will focus on the energy-capturing part of the light-dependent phase. However, a brief overview of the whole process of photosynthesis in plants will be given. There are some important differences between photosynthesis in plants, bacteria and algae, but the overview of plant photosynthesis below will suffice in giving the reader an idea of the overall aim and importance of photosynthesis. Where the differences between photosynthetic systems become relevant, they will be discussed in the text.

1.2.1 The light-dependent phase

The main outcome of the light-dependent phase is the synthesis of two important chemical compounds: adenosine triphosphate (ATP) and nicotinamide adenine dinucleotide phosphate (NADPH). The hydrolysis of ATP to adenosine diphosphate is highly exergonic (i.e., with copious release of free energy) [27]. The energy released by this hydrolysis reaction is used to perform the majority of energy-requiring processes in organisms. NADPH is a good reducing agent that provides the reducing power needed in the light-independent phase.

The electron transport chain

Each photosynthesising cell of a plant contains about one hundred [28] ellipsoidal ($\sim 2\,\mu$m by $5\,\mu$m) organelles called chloroplasts (Fig. 1.1).

Inside the chloroplast, a clear fluid called the stroma surrounds a closed, mem-

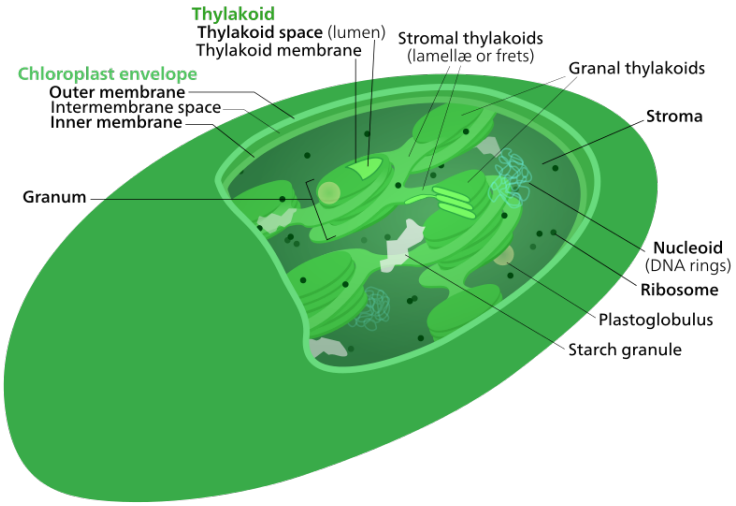

Figure 1.1: The chloroplast. ©User: Kelvinsong/ Wikimedia Commons/ CC-BY-SA 3.0.

branous structure. The light-dependent phase takes place in the membrane (called the thylakoid membrane) and the space enclosed by it (the thylakoid lumen). The thylakoid membrane forms structures resembling stacks of coins. These stacks, called grana, are connected by thin thylakoid membrane sheaths called lamellae. The thylakoid membrane consists of a lipid bilayer and houses the machinery of the light-dependent phase (Fig. 1.2).

The process of photosynthesis begins when a plant leaf is illuminated by light. A photon of this light travels into the chloroplast and gets absorbed by pigment molecules (mostly chlorophyll *a* molecules) in the pigment-protein complex called photosystem II. Inside PSII, the excitation is transported between pigment molecules until it is transferred to a special pair of pigment molecules called P680 (because the pair absorbs light at 680 nm). The excited state of P680 is often indicated by $P680^*$. The latter is a strong reducing agent and therefore readily transfers an electron to an acceptor called pheophytin (Ph). A charge transfer state $P680^+Ph^-$ is thus established [29]. The positive charge on $P680^+$ is neutralised by the transfer of an electron from water (see discussion on hydrolysis

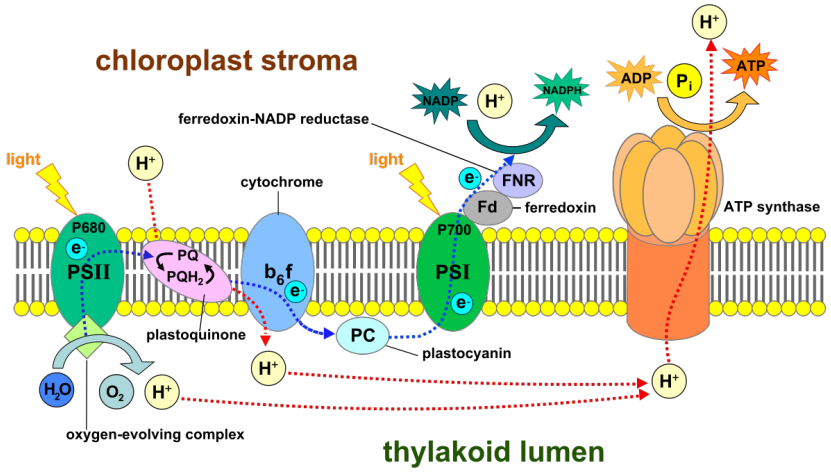

Figure 1.2: Cartoon of the thylakoid membrane with the most important machinery necessary for performing the light-dependent reactions. ©User: Somepics/ Wikimedia Commons/ CC-BY-SA 4.0.

below) and the Ph^- rapidly sponsors its extra electron to plastoquinone (PQ) [29]. By attaching two electrons, via this mechanism, and two protons from the stromal matrix to PQ, PQ is reduced to plastoquinol (PQH_2). Plastoquinol then binds to the thylakoid lumen side of an enzyme called cytochrome b_6f. Through a complex series of redox reactions called the Q-cycle, this enzyme catalyses the reduction of plastoquinone to plastocyanine and facilitates the release of protons (originally from the stromal matrix) into the lumen by plastoquinol [30].

During the reactions described above, PSI is continuously illuminated. By roughly the same mechanism as for PSII, the special pair of PSI (P700) is excited and a charge separation achieved. The positive $P700^+$ is neutralised by an electron from plastocyanine. The electron lost by P700 is used to reduce an iron-sulphur complex called ferredoxin on the stromal side of the thylakoid membrane. An enzyme called ferredoxin-$NADP^+$ reductase, which is also situated on the stromal side of the thylakoid membrane, then catalyses the reduction of $NADP^+$ to NADPH and the simultaneous oxidation of ferredoxin. The NADPH is released into the stroma

UNIVERSITEIT VAN PRETORIA
UNIVERSITY OF PRETORIA
YUNIBESITHI YA PRETORIA

for future use by the light-independent reaction.

The main result of the electron transport chain is therefore the absorption of light energy by the two photosystems (PSII and PSI) and the conversion of this energy to chemical reducing power by synthesising NADPH. An essential side effect of the electron transport chain is the pumping of H^+ across the thylakoid membrane. This leads to a proton gradient which is used in the synthesis of ATP (see below).

Hydrolysis

After the charge-separation $P680^+Ph^-$ in PSII is achieved, the negative charge is rapidly fed into the electron transport chain [31]. To neutralise the cation $P680^+$, an electron needs to be extracted from another species. In oxygenic photosynthesis, this electron donor turns out to be water, which is abundant in cells. $P680^+$ is the strongest known biological oxidising agent and is therefore able to oxidise water:

$$2\,H_2O \longrightarrow O_2 + 4\,H^+ + 4\,e^-\cdot$$

The above reaction is mediated by an enzyme called the oxygen-evolving complex (OEC). The exact role and mechanism of this complex are still unclear [32], but it is responsible for passing electrons, one at a time, to $P680^+$ [33]. The molecular oxygen produced by hydrolysis is a by-product of photosynthesis and is released into the atmosphere. Without this release of oxygen, however, the majority of life forms on earth would not exist! Oxygen is vital for the respiration of most types of organisms. Respiration is the process through which an organism acquires usable energy from food and can be considered a slow combustion reaction, therefore requiring oxygen.

UNIVERSITEIT VAN PRETORIA
UNIVERSITY OF PRETORIA
YUNIBESITHI YA PRETORIA

The synthesis of ATP

The photosynthetic hydrolysis of two water molecules passes four electrons to the electron transport chain and simultaneously releases four protons to the thylakoid lumen. For the four electrons released, the Q-cycle of cytochrome b_6f transfers eight protons from the stroma to the lumen. During the reduction of two ions of $NADP^+$ to NADPH, two protons from the stroma are bound. The net effect of these proton transfers is the addition of twelve protons to the lumen and the reduction of ten protons from the stroma. The chemi-osmotic [34] transfer of protons from the lumen back to the stroma through a trans-membrane enzyme called ATP-synthase, is what drives the synthesis of ATP.

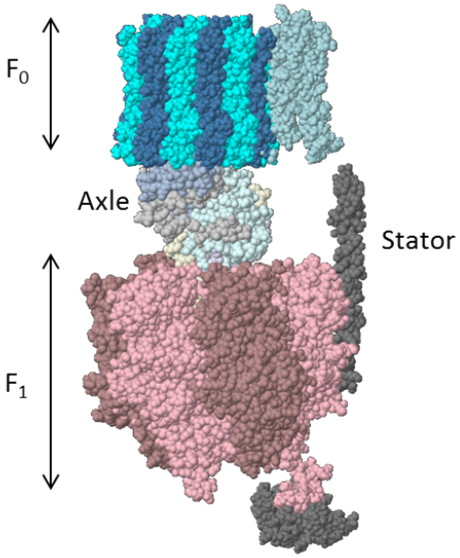

Figure 1.3: ATP-synthase with its main parts. Assembled with Jmol from PDB files 1L2P, 2A7U, 1E79, 1C17.

ATP-synthase consists of four main parts: the F_0 motor in the thylakoid membrane, the F_1 motor on the stromal side of the membrane, an axle connecting the two motors like a shaft and a stator connecting the sides of the motors. the F_0 motor consist of twelve subunits. Protons from the lumen attach, one at a time,

UNIVERSITEIT VAN PRETORIA
UNIVERSITY OF PRETORIA
YUNIBESITHI YA PRETORIA

to the F_0 motor and causes it to rotate through 30° per proton that attaches. This rotation is transferred to the axle and causes it to spin inside the F_1 motor. The F_1 motor consists of six subunits which form three dimers. The molecular structure of the axle is such that it causes specific configuration changes in the three dimeric subunits of the F_1 motor. These changes catalyses the addition of a phosphate functional group to adenosine diphosphate (ADP), thereby adding a large amount of energy to the compound. One full revolution of the F_0 motor yields three ATP molecules. The role of the stator is not yet clear, but it is thought that, together with the F_1 motor, it acts as a counter rotator to the F_0 motor [35].

Cyclic electron transport

During the linear electron transport chain discussed above, NADPH is produced. An alternative process in the light-dependent phase is the cyclic electron transport chain. During this process, ferredoxin reduces plastocyanine again [29], instead of reducing $NADP^+$. Plastocyanine then delivers its electron to PSI^+, which again leads to the reduction of ferredoxin. This cyclic process does not produce NADPH, but does pump protons into the lumen, thereby creating ATP. Through cyclic electron transport, the ratio of ATP to NADPH can be increased (the ratio created by non-cyclic electron transport is lower than what is needed by the light-independent phase).

1.2.2 The light-independent phase

The light-independent phase takes place in the stroma. During this phase, three-carbon molecules are manufactured that can easily be converted to sugars (like glucose) to provide the energy necessary for life. The process through which these three-carbon molecules are synthesised is called the Calvin-Benson-Bassham

cycle.

The Calvin-Benson-Bassham cycle

The Calvin-Benson-Bassham cycle (often simply called the Calvin cycle) consists of three main parts. First, carbon from CO_2 is fixated by reacting with another compound called ribulose bisphosphate (RuBP). In the second phase, glyceraldehyde-3-phosphate (G3P) is formed by reducing an intermediate species. G3P acts as the building block in many other metabolic pathways [36]. In the last phase, the starting material for the cycle is reproduced.

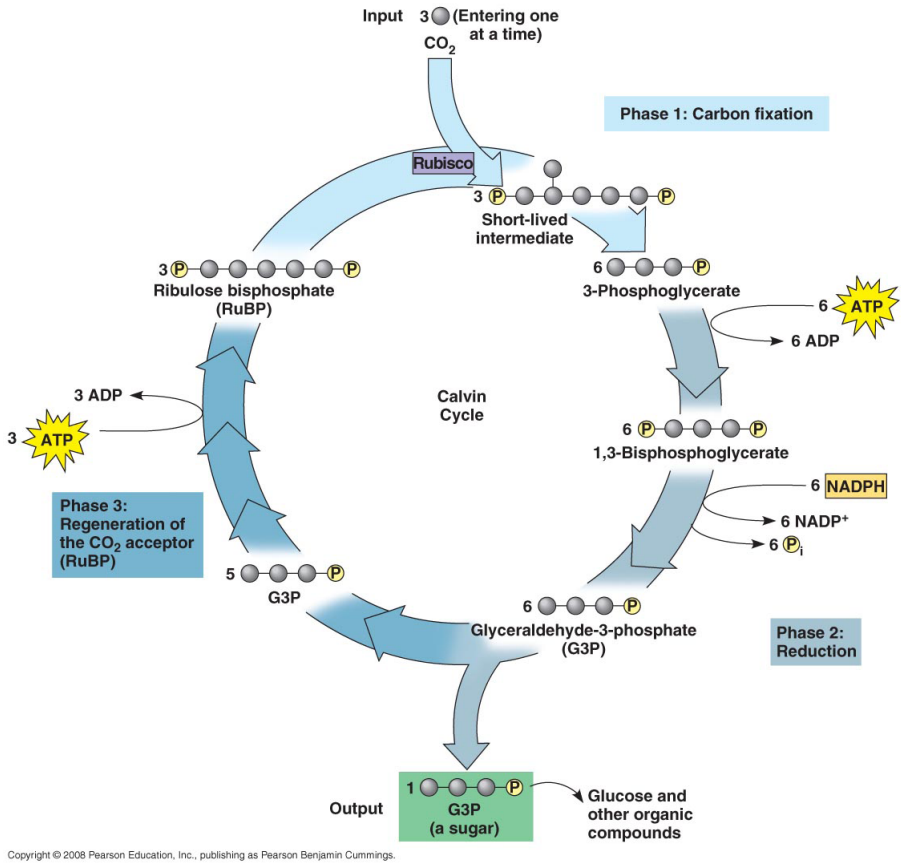

Figure 1.4: The Calvin cycle. CAMPBELL, NEIL A.; REECE, JANE B., BIOLOGY, 8th Edition, ©2008. Reprinted and electronically reproduced by permission of Pearson Education, Inc., Upper Saddle River, NJ.

UNIVERSITEIT VAN PRETORIA
UNIVERSITY OF PRETORIA
YUNIBESITHI YA PRETORIA

The Calvin cycle starts with the reaction of ribulose bisphosphate with CO_2. This reaction is catalysed by an enzyme called ribulose bisphosphate carboxylase (RuBisCo). Carbon dioxide reacts, one molecule at a time, in the stoichiometric ratio 1 : 1 with RuBP, but we will need to consider the reaction of three CO_2 molecules to have the correct total amount of carbon for the completion of the Calvin cycle. For three molecules of CO_2, the above reaction produces three molecules of a highly-unstable six-carbon compound which decomposes very rapidly to form six molecules of 3-phosphoglycerate, a three-carbon compound with one terminal phosphate group. ATP from the light-dependent phase is then used to phosphorylate these molecules and produce six molecules of 1,3-bisphosphoglycerate. The only difference between the reactant and product in this reaction is an extra phosphate functional group on the latter. Three carbon atoms that were originally in the gaseous phase are now fixated into this solid-phase compound.

In the second phase of the Calvin cycle, 1,3-bisphosphoglycerate is reduced by NADPH (fabricated during the light-dependent phase) into G3P.

During the third phase, five of the G3P molecules are used to regenerate the same amount of RuBP as was initially invested by expending another three molecules of ATP. The remaining molecule of G3P represents the three carbon atoms that were fixated from CO_2 and is exported to other parts of the organism.

1.3 Photosynthesis in other organisms

In this dissertation, we will use the relaxed definition of photosynthesis given in Henderson's Dictionary of Biology: photosynthesis is "the use of sunlight to power biosynthesis in living organisms" [37]. Processes in which ATP is synthesised but carbon is not fixated, are included in this definition.

UNIVERSITEIT VAN PRETORIA
UNIVERSITY OF PRETORIA
YUNIBESITHI YA PRETORIA

Just like plants, algae and cyanobacteria can oxidise water and therefore undergo *oxygenic* photosynthesis. The process of photosynthesis in these species is very similar to photosynthesis in plants (for discussions of photosynthesis in algae and cyanobacteria, see [38] and [39], respectively). Cyanobacteria are the only bacteria that use chlorophyll. Other photosynthesising bacteria use bacteriochlorophyll. Cyanobacteria are also the only bacteria that oxidise water. All other types of photosynthetic bacteria undergo anoxygenic photosynthesis

There are four known classes of anoxygenic bacteria: purple bacteria, green-sulphur bacteria, green non-sulphur bacteria and the gram-positive heliobacteria [40]. These bacteria use other reducing agents than water to photosynthesise. Purple bacteria use mainly H_2S and produce elemental sulphur as by-product.

1.4 Light harvesting in photosynthesis

To understand photosynthetic light harvesting, one has to appreciate the design of the harvesting machinery. In the light-dependent phase of plants, algae and cyanobacteria, light energy is absorbed by photosystems I and II. These two photosystems are significantly different from each other and from other natural photosystems. However, the physical principles underlying the light harvesting in the different photosystems are the same, and only the structure of photosystem II will therefore be discussed. Excitation dynamics in a general antenna complex will then be explained.

1.4.1 Structure of PSII

Except for the chlorosomes of green sulphur bacteria, all known photosystems consist of pigment molecules embedded in a complex assembly of protein struc-

UNIVERSITEIT VAN PRETORIA
UNIVERSITY OF PRETORIA
YUNIBESITHI YA PRETORIA

tures. PSII is a dimeric supercomplex where each monomer consists of a core and peripheral antenna complexes.

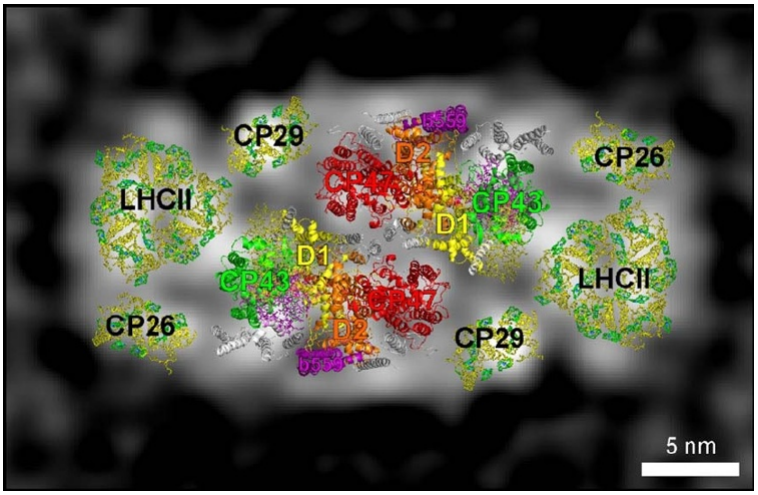

Figure 1.5: The proposed general structure of the PSII supercomplex. Here, the X-ray structures of antenna complexes are overlayed on the lumenal top view of the spinach PSII supercomplex, derived from electron microscopy and single particle analysis. The X-ray structures shown here, are that of the cyanobacterial core, spinach LHCII and structures adapted from the LHCII monomer for CP26 and CP29. Taken from Ref. [41] ©Elsevier (2006)

The core contains all the protein structures and cofactors (i.e., non-protein molecules) that are necessary for splitting water, creating a charge transfer state and reducing plastoquinone. The proteins D1 and D2 form a heterodimer that spans the thylakoid membrane and binds the special chlorophyll pair, the pheophytin molecules and the plastoquinones. D1 and D2 are often called the reaction centre proteins because they facilitate the splitting of water and creation of a charge separation. The reaction centre is surrounded by the core antennae chlorophyll-protein (CP) 43 and CP47 which provide conduits for excitation from the peripheral antenna complexes to the reaction centre [42] and are intimately related to the oxygen-splitting proteins [43]. The peripheral antenna complexes in plants consist of the minor antennae CP26, CP29 and CP24 (not shown in Fig. 1.5) and the major light-harvesting complex II (LHCII). Apart from acting

as energy bridges between LHCII and the reaction centre [44], the minor antenna complexes may also be involved in regulation of light harvesting: The reversible phosphorylation of CP29 is thought to influence antennae arrangement to increase damping in high intensity conditions, protecting the core from excess energy [45]. CP24 plays an important role in the electron transport chain [46], and CP26 is thought to facilitate grana stacking [47]. LHCII (Fig. 1.6) is a trimeric complex in which each monomer contains eight chlorophylls *a* (green), six chlorophylls *b* (cyan) and four carotenoids (yellow) [48]. The chlorophyll pigments are responsible for absorbing sunlight while the carotenoids are mainly responsible for protecting the light-harvesting apparatus from excess excitation (although they also absorb energy for the reaction centre) [49].

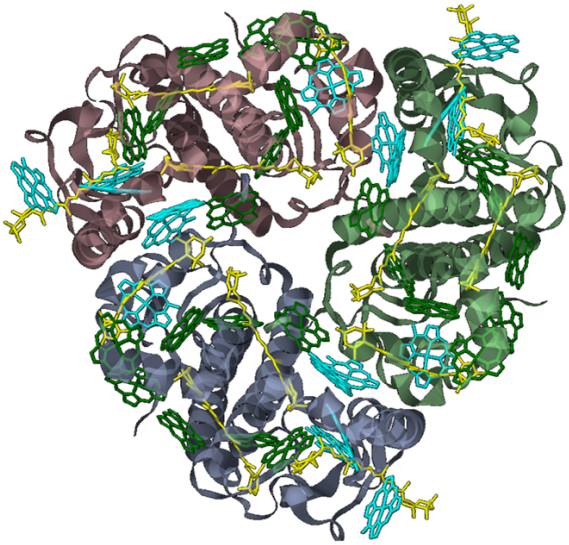

Figure 1.6: Light-harvesting complex II. Made by Jmol from PDB file 2BHW.

UNIVERSITEIT VAN PRETORIA
UNIVERSITY OF PRETORIA
YUNIBESITHI YA PRETORIA

1.4.2 The fate of an excitation

When light is shone on an antenna complex, clusters of pigment molecules (or individual pigment molecules) are excited. These excitations are transferred from cluster to cluster within a light-harvesting complex or between different complexes. In this way, light energy that was initially absorbed by the antenna complex is ultimately transferred to the reaction centre. The average time it takes an excitation to reach a reaction centre is on the order of tens of picoseconds [50] and the quantum efficiency (i.e., probability of the energy of an absorbed photon to manifest in a charge-separation state) of the energy transfer is very near to 100% [51]. How this fast transfer rates and high efficiency is achieved has sparked much research interest (this dissertation included).

The density of pigment molecules in photosynthetic light-harvesting complexes is remarkable: In solution, and in many artificial systems, chlorophyll fluorescence is significantly suppressed when the chlorophyll concentration is comparable to the concentration in chloroplasts [23, 52]. No such suppression is seen in the fluorescence of the chloroplast [52]. This means that the lifetime of excited states (which determine the time an excitation has to reach the reaction centre) is not influenced by pigment aggregation in light-harvesting complexes [53]. This high working-concentration can be achieved because of precise arrangement of pigment molecules by the protein scaffold. The positions and orientations of pigment molecules afforded by the protein also optimises energy transfer [54].

To understand this optimisation, notice that pigment molecules in close proximity may interact with one another (this interaction, or coupling, will be explained in Section 2.2). Due to the inter-pigment coupling, the energy landscape of the quantum states that are realised after excitation by light is very different from that of isolated pigment molecules. Instead of exciting only one pigment molecule, a

UNIVERSITEIT VAN PRETORIA
UNIVERSITY OF PRETORIA
YUNIBESITHI YA PRETORIA

coherent superposition of the excited states of different pigments are formed upon illumination of an antenna complex (see Section 2.5). An excitation in a dense cluster of pigment molecules is therefore delocalised over the whole cluster. Such delocalised excitations are called excitons.

The formation of excitons in light-harvesting systems has two important beneficial features. Firstly, because of delocalisation of excitation, fewer paths have to be explored when the excitation diffuses to the reaction centre. Secondly, delocalisation prevents excitation from getting trapped in energy wells (that may be present due to crystal defects [54]).

The electronic degrees of freedom are influenced by the large number of vibrational modes in the protein and in the pigment molecules themselves. In Section 2.4, we will see how the excitation dynamics are influenced by these vibrations. In this dissertation, we will investigate these dynamics—especially in the special case when the interaction with vibrations is small.

In the next chapter, we give a qualitative description of the mechanisms underlying exciton relaxation. We then derive the Redfield equation, which gives a good description of exciton dynamics in the weak relevant system–bath coupling limit, in Chapter three. In Chapter four, we describe a system containing multiple excitations. A computer program that simulates Redfield dynamics in single-exciton and two-exciton systems is described in Chapter five. In Chapter six, we illustrate and discuss the Redfield dynamics in three example systems.

UNIVERSITEIT VAN PRETORIA
UNIVERSITY OF PRETORIA
YUNIBESITHI YA PRETORIA

Chapter 2

Introduction to theory

2.1 Overview

It may be surprising to many physicists that quantum mechanics beyond typical quantum chemistry is needed to fully describe photosynthetic light harvesting. On the molecular level, plants are disordered systems with many fluctuating degrees of freedom (at physiological temperatures)—an environment with which we do not usually associate nontrivial quantum effects. In reality, however, even though light-harvesting complexes are intricate, the protein scaffold provides the pigment molecules with positions and orientations that permit quantum coherence between pigment molecules to exist. The important implications of this coherence to photosynthetic light harvesting will be discussed in Section 2.5.

Because of their complexity, the pigment-protein complexes have a very large number of vibrational modes. These vibrations collectively act as thermal reservoirs, exchanging energy with the electronic degrees of freedom of the pigments. The energy exchange between the electronic degrees of freedom and the reservoir influences the excitation dynamics and needs to be taken into account. In practice,

UNIVERSITEIT VAN PRETORIA
UNIVERSITY OF PRETORIA
YUNIBESITHI YA PRETORIA

the light-harvesting systems are far too big and far too complex to allow calculation of the dynamics of all degrees of freedom, and some effective description of the environment has to be employed. A description of the excitation energy transfer dynamics therefore needs to be both quantum mechanical (to account for quantum coherence) and statistical (to account for the relaxation effects of the large, complex environment). We achieve this by treating electronic excitation as a small quantum subsystem interacting with a much larger environment. The total system evolves unitarily in time and can be described by identities such as the Liouville equation. By making statistical assumptions about the environment, these identities can be cast into forms that permit calculation of excitation transfer dynamics (see Chapter 3).

To this end, let us divide the total system in two parts [55]: a subsystem (which we call the relevant system[1]) containing only the electronic degrees of freedom, and a subsystem (which we call the bath) containing all other degrees of freedom.

The total Hamiltonian can then be written in the form

$$H = H_{RS} + H_B + H_I, \tag{2.1}$$

where H_{RS} describes the relevant system, H_B describes the bath and H_I describes the interaction between the relevant system and the bath.

Below, we elaborate on each of these partitions.

[1]The word "system" can cause confusion. We will use the term "relevant system" for the electronic degrees of freedom and "bath" for all other degrees of freedom such that the union of relevant system and bath evolves unitarily in time. We will reserve the term "system" exclusively for this union.

UNIVERSITEIT VAN PRETORIA
UNIVERSITY OF PRETORIA
YUNIBESITHI YA PRETORIA

2.2 The relevant system

Each of the pigment molecules in a light-harvesting complex can be regarded as a two-level system with a ground state and an excited state [56]. Associated with each pigment molecule is a transition dipole moment describing the change in charge density upon excitation of the pigment molecule. The transition dipole moments of different molecules interact with one another and different pigment molecules are therefore *coupled*. The pigments themselves don't have any net charge, and the dominant Coulomb interaction between two pigment molecules is therefore described by the dipole-dipole potential of the two transition dipole moments. The strength of the coupling depends on the distance and relative orientations of the pigment molecules [57]. The interaction potential energy between two molecules with transition dipole moments $\vec{\mu}_1$ and $\vec{\mu}_2$ is:

$$V_{12} = \frac{\vec{\mu}_1 \cdot \vec{\mu}_2 - 3(\vec{\mu}_1 \cdot \hat{R})(\vec{\mu}_2 \cdot \hat{R})}{R^3}, \tag{2.2}$$

where R is the distance between molecules 1 and 2 and $\hat{R}$ is the normalised separation vector. The Hamiltonian describing an aggregate of pigment molecules in which exactly one excitation is present is therefore:

$$H_{el} = E_g \left|g\right\rangle \left\langle g\right| + \sum_{i=1}^{N} E_{e_i} \left|e_i\right\rangle \left\langle e_i\right| + \sum_{i \neq j}^{N} V_{ij} \left|e_i\right\rangle \left\langle e_j\right|, \tag{2.3}$$

where the first term is the ground state energy of the relevant system (the energy of the aggregate when all pigment molecules are in their ground states) and the second term is a sum of single-excitation energies (only molecule i is in its excited state). The last term represents the dipole coupling between different pigment molecules. Eq. 2.3 is not exactly equal to the relevant subsystem Hamiltonian (which, as we will see in the next section, still requires a bath-reorganisation contribution).

UNIVERSITEIT VAN PRETORIA
UNIVERSITY OF PRETORIA
YUNIBESITHI YA PRETORIA

Strictly speaking, we should multiply (i.e., take the tensor product) with the bath identity operator on the right of Eq. 2.3. This operator acts as identity operator on the bath degrees of freedom. To keep equations from getting cluttered and losing their essence, multiplication with a bath identity operator will be implied throughout this dissertation if only relevant system-dependence is shown for full-system operators. Similarly, if only bath dependence is shown, multiplication with a relevant system identity operator will be implied.

In light harvesting under natural conditions, the rate of exciton formation (through photon absorption) is often so low that only one exciton is present at any moment in time. In these cases, Eq. 2.3 is accurate. If a multiple-exciton description is required, Eq. 2.3 can easily be extended (see chapter 4).

2.3 The bath

The bath Hamiltonian has a very large number of contributors. Intra-molecular interactions in the pigments and in the protein molecules, inter-molecular potentials between two pigment molecules, between a pigment molecule and the protein environment, and between different protein subunits, all contribute to the potential energy part. The kinetic part of the bath Hamiltonian describes the movement of the many nuclei and electrons.

We want to describe the dynamics of the relevant system and are not interested in the dynamics of the bath, except where those dynamics influence the relevant system. We will see in Chapter 3 that the influence of the bath enters the equation of motion for the relevant system only through statistical quantities called bath correlation functions. These quantities can be extracted from experimentally obtained optical spectra [58], and no microscopic knowledge of the bath is

necessary. When developing a theoretical approach, however, at least some microscopical consideration of the bath is required for calculating the correlation functions. Apart from allowing calculation of correlation functions, microscopic knowledge of the bath also gives one some physical insights into the effect of the bath on the system.

One theoretical approach that is often used is the following. Instead of treating H_B exactly, by describing all of the numerous and complex contributions in the first paragraph of this section, the actual bath is substituted with an effective bath having almost the same effect on the system. This effective bath is composed of the kinetic and potential energy parts of the normal harmonic oscillator modes for all of the above contributions. The effective bath is chosen such that its spectral density corresponds to the spectral density of the actual bath. A commonly used effective bath consists of an infinite number of independent quantum harmonic oscillators [59]. These harmonic oscillators are coupled linearly (see below) to the relevant subsystem. As we will see later, this harmonic bath determines the relaxation of the relevant system.

2.4 Interaction of the relevant system with the bath

We will now consider the interaction between the relevant system and one harmonic oscillator mode of the environment and then extend the ideas to account for an arbitrary (even infinitely many) environmental oscillators.

Consider an isolated pigment molecule consisting of two identical subunits. For comparison with Eq. 2.3, we will call this molecule i.

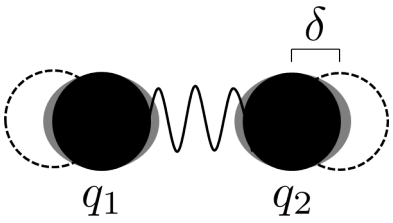

Figure 2.1: A pigment molecule consisting of two identical subunits. The coordinates of the two subunits measured on the same coordinate axis are given by q_1 and q_2, and δ is the equilibrium shift in each of these coordinates upon excitation of the molecule.

One of the vibrational modes of the molecule constitutes stretching and contracting along the axis connecting the two subunits. Let's consider an effective coordinate $Q = q_1 - q_2$. The potential energy causing the oscillation is now quadratically dependent on Q. Let the minimum of this potential be indicated by the black circles when the molecule is in its ground state. Suppose that the structure of this molecule in its excited state is such that the equilibrium position of each subunit is shifted a distance δ outwards. The potential minimum (in coordinate Q) is therefore shifted by $d = 2\delta$. Because of the large masses of the subunits, one can assume that the oscillations happen on a much slower timescale than the transition from the ground to the excited state in molecule i (adiabatic approximation). To excite molecule i from the vibrational ground level of its electronic ground state, one therefore has to apply more excitation energy than the energy difference $E_{e_i} - E_g$ in Eq. 2.3. The energetics accompanying the electronic excitation is depicted in Fig. 2.2. The parameter d in Fig. 2.2, which is equal to 2δ in Fig. 2.1, describes how strongly the relevant system is perturbed by (or *coupled* to) the oscillation. This parameter will be useful later again.

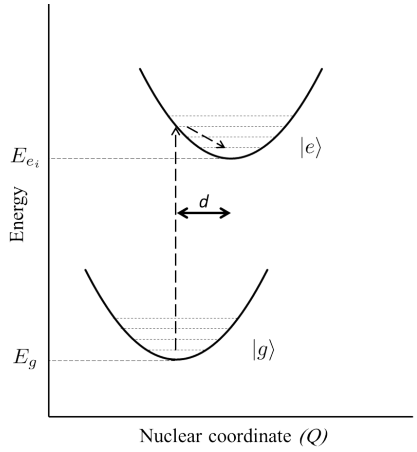

Figure 2.2: The harmonic oscillator potentials corresponding to the ground and excited states of a pigment molecule with two subunits. As indicated by the dashed line arrows, the molecule is excited to a higher vibrational level of the electronic excited state, before relaxing to the ground vibrational level. The parameter d is directly related to the coupling strength between electronic excitation and the molecular vibration.

In the same way as was discussed above, the relevant system is influenced by numerous inter- and intra-molecular vibrations. We want to have a collective description of the interaction of all of these vibrations with the relevant system. Consider the Hamiltonian describing all of the oscillators and their individual coupling to the relevant system:

$$H_{osc} = \left(T + \sum_{i=1}^{N} \sum_{k} \frac{\hbar\omega_{ki}}{2} q_{ki}^2\right) |g\rangle\langle g| + \sum_{i=1}^{N} \left(T + \sum_{k} \frac{\hbar\omega_{ki}}{2} (q_{ki} - d_{ki})^2\right) |e_i\rangle\langle e_i|, \quad (2.4)$$

with T the kinetic energy of the nuclei, ω_{ki} and q_{ki} the frequency and coordinate, respectively, of the k^{th} harmonic oscillator coupled to molecule i, and d_{ki} the amount by which a harmonic oscillator is perturbed by the excitation of a pigment molecule.

From Eqs. 2.3 and 2.4, we can now separate the terms that are static in bath degrees of freedom or in electronic degrees of freedom into a relevant system

Hamiltonian and bath Hamiltonian respectively:

$$H_{RS} = E_g \left|g\right\rangle \left\langle g\right| + \sum_{i=1}^{N} \left(E_{e_i} + \sum_k \frac{\hbar\omega_{ki}}{2} d_{ki}^2 \right) \left|e_i\right\rangle \left\langle e_i\right| + \sum_{i,j=1}^{N} V_{ij} \left|e_i\right\rangle \left\langle e_j\right| \tag{2.5}$$

and

$$H_B = T + \sum_{i=1}^{N} \sum_k \frac{\hbar\omega_{ki}}{2} q_{ki}^2. \tag{2.6}$$

The term $\sum_k \frac{\hbar\omega_{ki}}{2} d_{ki}^2$ in Eq. 2.6 is called the reorganisation energy of the bath. This energy is lost when the bath relaxes to the vibrational ground state following an electronic excitation (which is always vertical; see Fig. 2.2). In the rest of this dissertation, we will include the reorganisation energy in the excitation energy E_{e_i}.

The Hamiltonian for the interaction between the relevant system and the bath depends on both system and bath operators and can be written as:

$$H_I = \sum_{i=1}^{N} \sum_k \hbar\omega_{ki} q_{ki} d_{ki} \left|e_i\right\rangle \left\langle e_i\right|. \tag{2.7}$$

Notice that the interaction Hamiltonian is linear both in bath operators (the q_k) and relevant system operators (the $\left|e_i\right\rangle \left\langle e_i\right|$).

2.5 Qualitative description of excitation dynamics

We are now in a position to discuss, qualitatively, what happens to an excitation in a light-harvesting complex.

In Section 1.4.2, the general characteristics of an excitation in a photosynthetic light-harvesting complex were discussed. We will now elaborate on that description by using the ideas presented in this chapter.

UNIVERSITEIT VAN PRETORIA
UNIVERSITY OF PRETORIA
YUNIBESITHI YA PRETORIA

When a photon is absorbed by a light-harvesting complex, a group of pigment molecules are excited simultaneously. This simultaneous excitation is made possible by the close proximity, and therefore strong coupling, of pigment molecules to one another. In the language of quantum mechanics, a superposition (or linear combination) of the excited states of individual molecules is formed. Due to the quantum nature of light absorption, one photon can excite only one pure state and the energy of this *coherent superposition* of molecules is therefore equal to the energy of the photon that was absorbed. Since the superposition state has to have a definite energy, it should be an eigenstate of the total Hamiltonian. The part of the bath described by Eq. 2.6 cannot be excited directly by light and the excited state will consequently be, almost exactly, an eigenstate of the system Hamiltonian[2]. These eigenstates are called excitons since they are, fundamentally, electron-hole bound states. In photosynthetic light harvesting, the electron and hole are located on the same pigment molecule, and photosynthetic excitons are therefore of the Frenkel type [57].

If the relevant system were closed, the eigenstate that was excited upon light absorption would evolve unitarily and the state's population would remain constant. Of course, the system is not isolated, and the environment plays a crucial role in transporting absorbed energy through the light-harvesting complex. To understand the role of the environment, it is important to note that the excitons couple, like individual pigments, linearly to the oscillator bath. Fig. 2.2 is therefore still a valid representation of excitation from the ground state if we let $|e\rangle$ denote an exciton state and Q a collective bath coordinate. As explained in Section 2.4, the electron densities of pigments involved in an exciton state shift very rapidly to the electron density of the excited state when an exciton is created. The nuclei, on

[2]In reality, the many vibrations in the bath cause small fluctuations in the energy difference between the ground state and excited states. These states are consequently not exact eigenstates of the system Hamiltonian.

UNIVERSITEIT VAN PRETORIA
UNIVERSITY OF PRETORIA
YUNIBESITHI YA PRETORIA

the other hand, change their positions much more slowly—so slow that they are essentially still in the same positions directly after excitation as they were before. Because of this slow change, a non-ground vibrational level of the exciton state gets populated first before the system relaxes slowly to the lowest vibrational level of the exciton state.

In reality, not all excitons in an ensemble are in the lowest vibrational level. In Section 3.2, we will assume that the bath is always in thermal equilibrium. The populations of different vibrational levels therefore conform to the Boltzmann distribution. In this distribution, the probability for the system to be in the i^{th} vibrational level, with energy ε_i, is given by

$$p_i = \frac{e^{-\varepsilon_i/kT}}{\sum_{i=0}^{\infty} e^{-\varepsilon_i/kT}}. \tag{2.8}$$

At room temperature (i.e., the temperature at which photosynthesis normally takes place), the lowest vibrational level has by far the highest population, but vibrational levels with higher energy play an important role in describing the excitation dynamics of a system. To understand this, consider two exciton states α and β, where the electronic transition energy of α is higher than that of β (see Fig. 2.3)

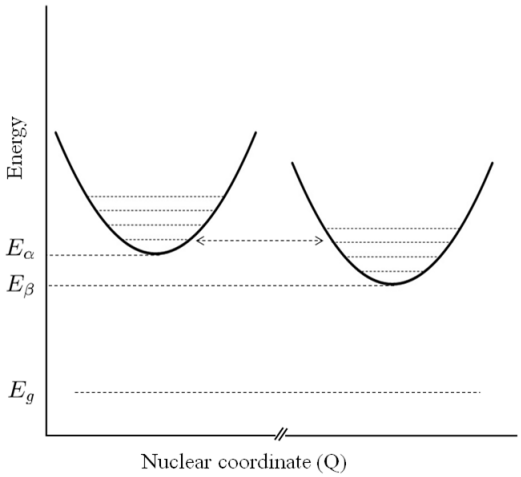

Figure 2.3: The harmonic oscillators coupled to the excitons α and β. For simplicity, the ground state oscillators are not shown. Q represents a collective nuclear coordinate.

Excitation can be transferred between exciton states α and β only if the energy lost by α as it falls to the electronic ground state[3] equals the energy required to excite β to the electronic excited state. In Fig. 2.3, exciton α in its lowest (zeroth) vibrational level can fall to the (zeroth) vibrational level of the electronic ground state and simultaneously excite β from this level to the second vibrational level of its electronic excited state. Of course, it is also possible for α to fall to a higher vibrational level of the electronic ground state and excite β to a lower vibrational level. Many such possible de-excitation–excitation possibilities exist in real-world systems and the overlap of an emission spectrum (for the excitation donor) and absorption spectrum (for the acceptor) determines the rate of excitation transfer. In the rest of this dissertation, we will think of the excitation being *transferred* between exciton states and will not describe the mechanism of simultaneous excitation and de-excitation every time.

In Fig. 2.3, energy can only be transferred to α from the second vibrational level of β. Assuming that the density of vibrational states for the two excitons are equal,

[3]It is not correct to speak about an exciton "falling to the ground state" or "being excited": an exciton can only be created or annihilated. Since a correct description will be much longer and technical, we will not be pedantic.

UNIVERSITEIT VAN PRETORIA
UNIVERSITY OF PRETORIA
YUNIBESITHI YA PRETORIA

the probability of transferring excitation from β to α, relative to the probability of transferring excitation from α to β can be obtained from Eq. 2.8:

$$\frac{p_2}{p_0} = e^{(\varepsilon_0 - \varepsilon_2)/kT}. \tag{2.9}$$

In the absence of fluorescence or other decay channels, this transfer of excitation between states α and β would occur indefinitely. If we had a very large number of identical systems, an equilibrium will be reached in which the numbers of excitons α (N_α) and β (N_β) will remain constant. This equilibrium will be reached when $\frac{N_\alpha}{N_\beta} = e^{(\varepsilon_0 - \varepsilon_2)/kT}$ (i.e., when the *net* transfer rates are zero).

2.6 Bases for describing excitation dynamics

In order to evaluate the excitation dynamics determined by Hamiltonians 2.5, 2.6 and 2.7 in a real-world system, we need to express these Hamiltonians in a suitable basis. Two bases seem to be natural choices:

Site basis

The site basis is the set of states $\{|e_i\rangle\}$, where the system is in state $|e_i\rangle$ when only the i^{th} pigment molecule is excited and all other pigments are in their ground states. The site basis is orthonormal: for a system in the pure state $|e_i\rangle$, the population of that site ($\langle e_i | e_i \rangle$) is one and the populations of all other states are zero. One can therefore write $\langle e_j | e_i \rangle = \delta_{ji}$.

Since the site energies of pigment molecules and couplings between them can be determined from spectroscopy and quantum-chemistry computations, the site basis is the natural basis for expressing the Hamiltonian.

Eigenbasis

Any complete set of eigenvectors of the system Hamiltonian forms an eigenbasis. Unlike the site basis, an orthonormal eigenbasis does not necessarily consist of a unique set of vectors. One can find an orthonormal eigenbasis by diagonalizing the site-basis system Hamiltonian. The matrix A that satisfies $A^{-1}H_{RS}^{\text{site basis}}A = H_{RS}^{\text{diagonal}}$ contains a complete set of eigenvectors as columns. The diagonal entries of H_{RS}^{diagonal} are the eigenvalues of H_{RS} and the columns of A (in order) are the eigenvectors of the corresponding eigenvalues. In light-harvesting complexes, the excitons occupy the eigenstates of the system Hamiltonian and the eigenbasis is therefore also called the exciton basis.

2.7 Most common formalisms for computing excitation dynamics

2.7.1 Förster resonance energy transfer

Förster resonance energy transfer (FRET) describes the nonradiative transfer of energy from an excited chromophore (pigment molecule) to a non-excited chromophore through dipole-dipole coupling. Delocalisation of excitation over multiple chromophores is not allowed in FRET. The efficiency of transfer depends on the distance between the chromophores, the relative orientation of their transition dipole moments and the spectral overlap of the donor's emission spectrum and the acceptor's absorption spectrum. FRET is an approximate theory that works well for chromophores on which excitation is localised. This is the case when the inter-chromophore coupling is weak relatively to the coupling between chromophores and the environment. This regime is called the weak resonance-coupling limit. In

UNIVERSITEIT VAN PRETORIA
UNIVERSITY OF PRETORIA
YUNIBESITHI YA PRETORIA

this limit, fluctuations from the environment are so strong that any already-weak inter-chromophore coupling is annihilated. In almost all light-harvesting systems, the coupling between chromophores is not weak and excitation is delocalised over several pigments. The predictions from FRET therefore differ significantly from what is observed experimentally. An adjusted version of FRET, called generalised Förster theory, allows for strong inter-chromophore coupling in a cluster of chromophores with weak coupling between the clusters. A strong resonance-coupling limit approach like Redfield theory (Section 2.7.2) has to be applied when calculating transfer dynamics within such clusters, however.

2.7.2 Redfield theory

The Redfield equation, which determines the time-evolution of the relevant system in the Redfield theory framework, will be derived in Chapter 3. The Redfield theory is a second-order perturbation theory in which the interaction Hamiltonian is handled as a perturbation. This theory assumes strong inter-chromophore coupling relatively to the chromophore-environment coupling. Redfield theory is therefore applicable in the opposite limit than FRET. Most of the predictions of Redfield theory agree well with what is observed experimentally in light-harvesting systems (see Chapter 6). Discrepancies between the theoretical prediction and experimental observation can be significant enough, however, to warrant the use of more accurate methods.

2.7.3 Modified Redfield theory

All ideas in this section were taken from Ref. [60]. In modified Redfield theory, which was first derived by Zhang et al. [61], the diagonal part of the interaction Hamiltonian in the exciton basis $\{|k\rangle\}$ is handled non-perturbatively. The off-

diagonal elements can be written as [60]

$$H' = \sum_{k \neq k'} |k\rangle H^I_{kk'} \langle k'| , \tag{2.10}$$

and their magnitudes depend on two factors: the overlap of the two exciton wave functions and the coupling of the pigments to the bath. In systems for which the average overlap between different exciton wave functions is small, the perturbation approach (on the off-diagonal elements of H') is valid even for strong coupling to the bath. Systems for which the average exciton wave functions overlap is small include systems with high static disorder or those in which the spectra of the chromophores are well-separated. Both of these characteristics are often found in light-harvesting systems.

2.7.4 Reduced hierarchy equation approach

The Reduced hierarchy equation approach is a non-perturbative approach that can be used to calculate excitation dynamics over all ranges of pigment-environment coupling strength and reduces to the Redfield and Förster formalisms in their respective limits [62]. This approach is computationally intensive [63, 64] and the theory not as perspicuous as Redfield theory.

UNIVERSITEIT VAN PRETORIA
UNIVERSITY OF PRETORIA
YUNIBESITHI YA PRETORIA

Chapter 3

Redfield formalism

Excitation dynamics in molecular aggregates are often described by making use of the Redfield formalism. In this chapter, we derive the Redfield equation, which predicts excitation dynamics in this formalism. To this end, we first introduce some preliminary concepts necessary for the derivation.

3.1 Preliminary concepts

3.1.1 The density matrix

An example

Not all quantum states can be expressed as wave functions. Pure states (which can be expressed as wave functions) are always eigenvectors of Hermitian operators.

In reality, systems often consist of a large number of particles that occupy different pure states with a given classical distribution. These *mixed* quantum states are not single wave vectors in any Hilbert space and subsequently have to be expressed statistically.

UNIVERSITEIT VAN PRETORIA
UNIVERSITY OF PRETORIA
YUNIBESITHI YA PRETORIA

To see how we express these states, let us suppose that we have a large ensemble of systems and that the only difference between the systems is that half of the ensemble is initially in the pure state $|\phi\rangle$ and the other half in the pure state $|\psi\rangle$. Before performing any measurements, we do not know which members of the ensemble are in which state. Suppose also that the pure states can be expressed as $|\phi\rangle = c_a|a\rangle + c_b|b\rangle$ and $|\psi\rangle = c_d|d\rangle + c_e|e\rangle$. When we make a measurement of the observable, say $\hat{A}$, that has eigenvectors $|a\rangle, |b\rangle, |d\rangle$ and $|e\rangle$, we find that in half of the cases (for the members of the ensemble which were in state $|\phi\rangle$) we obtain result a and b with probability c_a^2 and c_b^2 respectively. Overall, we obtain a, b, d and e with probabilities $\frac{1}{2}c_a^2$, $\frac{1}{2}c_b^2$, $\frac{1}{2}c_d^2$ and $\frac{1}{2}c_e^2$ respectively.

How can we characterise this system in the eigenbasis of $\hat{A}$? We should certainly report the probability of obtaining a certain eigenvalue, but this information is not sufficient. To predict the evolution of the ensemble, for example, we should also know that $|a\rangle$ and $|b\rangle$ cooperate through a linear combination to form the pure state $|\phi\rangle$. We can quantify this cooperation by calculating the quantity $c_a c_b^* = \langle a|\phi\rangle\langle\phi|b\rangle$. For $c_a, c_b \in \mathbb{R}$, this quantity has a maximum value when $|c_a| = |c_b|$ (i.e., maximum cooperation between states $|a\rangle$ and $|b\rangle$) and is zero when either $c_a = 0$ or $c_b = 0$ (i.e., no cooperation at all). We can also extract phase information from this quantity: If $c_a c_b^* = \frac{i}{2}$, we can infer that c_a is leading by $e^{\frac{i\pi}{2}}$. We can condense all of this information into a matrix, which we call the density matrix. We put the probabilities of obtaining eigenvalues on the diagonal and fill in the rest of the matrix with the cooperation factors:

$$\rho = \begin{bmatrix} \frac{1}{2}c_a^2 & c_a c_b^* & 0 & 0 \\ c_b c_a^* & \frac{1}{2}c_b^2 & 0 & 0 \\ 0 & 0 & \frac{1}{2}c_d^2 & c_d c_e^* \\ 0 & 0 & c_e c_d^* & \frac{1}{2}c_e^2 \end{bmatrix}. \tag{3.1}$$

Calculation of the density matrix in general

The density matrix contains all information we can possibly extract from the system. In general, we can construct a density matrix for any state (both pure and mixed) by the following method. Suppose a quantum system can be found in state $|\psi_1\rangle$ with probability p_1, in state $|\psi_2\rangle$ with probability p_2, in state $|\psi_3\rangle$ with probability p_3 etc. We then define the density operator as

$$\hat{\rho} = \sum_i p_i |\psi_i\rangle \langle\psi_i| . \tag{3.2}$$

The (density) matrix associated with this operator is calculated by projecting the operator to a basis set $\{|b_n\rangle\}$:

$$\rho_{kl} = \sum_i p_i \langle b_k | \psi_i\rangle \langle\psi_i | b_l\rangle . \tag{3.3}$$

The diagonal elements of the density matrix are the populations of the basis vectors (the expectation value of that basis state) and the off-diagonal elements are the coherences between different basis vectors (indicating the average amount of quantum coherence between them). All entries of the density matrix depend on the basis in which it is expressed and it is not always trivial to see whether a state is pure.

Properties of the density matrix

To determine whether a state is pure, we calculate the trace of the density matrix. The trace is simply the sum of all the diagonal elements. The state represented by a density matrix is pure if and only if $\mathrm{tr}(\rho^2) = 1$. In the next chapter, we'll also

UNIVERSITEIT VAN PRETORIA
UNIVERSITY OF PRETORIA
YUNIBESITHI YA PRETORIA

make use of the cyclic property of the trace operation:

$$\mathrm{tr}(\hat{A}\hat{B}\hat{C}) = \mathrm{tr}(\hat{C}\hat{A}\hat{B}) = \mathrm{tr}(\hat{B}\hat{C}\hat{A}) \tag{3.4}$$

The density matrix gives us an easy way of calculating the expectation value of an operator. If the system is in the state described by ρ then, for an operator $\hat{A}$ acting on the system,

$$\langle \hat{A} \rangle = \mathrm{tr}(\hat{A}\hat{\rho}). \tag{3.5}$$

3.1.2 Interaction picture

There are three reference frames ("pictures") that are often used in quantum mechanics: the Schrödinger picture in which the state vectors (or basis vectors in the case of mixed states) carry all time-dependence, the Heisenberg picture in which states are stationary and operators carry the time-dependence, and the interaction (Dirac) picture in which both state vectors and operators evolve in time. The interaction picture is useful when we want to investigate the time-evolution due to an interaction between two subsystems. One can think of the interaction picture as a reference frame that moves through phase space in such a way that we only observe the tugs and pulls on the system due to the interaction. The interaction picture also has some mathematical advantages that will be useful later.

For defining operators and states in the interaction picture, we partition the total Hamiltonian in two parts: $\hat{H}_0 = \hat{H}_{RS} + \hat{H}_B$ and $\hat{H}_I$ (see Eq. 2.1). We then define the interaction picture operators and states from their Schrödinger counterparts:

$$|\psi(t)\rangle^I = e^{i\hat{H}_0 t/\hbar} |\psi(t)\rangle^S \tag{3.6}$$

and

$$\hat{A}^I(t) = e^{i\hat{H}_0 t/\hbar}\hat{A}^S(t)e^{-i\hat{H}_0 t/\hbar}. \tag{3.7}$$

By substituting definition 3.6 into Eq. 3.2, it is easy to see that the density operator does indeed transform according to Eq. 3.7.

One can transform between the interaction picture and Schrödinger picture by using the Heisenberg equation,

$$\frac{d}{dt}\hat{A}(t) = \frac{i}{\hbar}\left(\hat{H}_0\hat{A}(t) - \hat{A}(t)\hat{H}_0\right) + e^{i\hat{H}_0 t/\hbar}\left(\frac{\partial \hat{A}}{\partial t}\right)e^{-i\hat{H}_0 t/\hbar}. \tag{3.8}$$

In the following sections we will denote the density operator as $\hat{\rho}'(t)$ in the interaction picture. For other operators, we will indicate time-dependence explicitly, like in $\hat{A}(t)$, if and only if these operators are in the interaction picture[1]. We will also drop the operator hat in the next section.

3.1.3 Liouville-von Neumann equation

We can easily write down the time-dependence of the density matrix from Eq. 3.2:

$$\begin{aligned}\rho(t) &= \sum_i p_i e^{-iHt/\hbar}\left|\psi_i\right\rangle\left\langle\psi_i\right|e^{iHt/\hbar} \\ &= e^{-iHt/\hbar}\sum_i p_i\left|\psi_i\right\rangle\left\langle\psi_i\right|e^{iHt/\hbar} \\ &= e^{-iHt/\hbar}\rho e^{iHt/\hbar}.\end{aligned}$$

The first derivative of this equation is known as the Liouville-von Neumann equa-

[1]The full density matrix evolves unitarily in time, but the reduced density matrix in Section 3.2 does not. Only indicating time-dependence explicitly will therefore not always be a sufficient indication that the density matrix is in the interaction picture.

tion:

$$\frac{\partial}{\partial t}\rho = -\frac{i}{\hbar}[H,\rho]. \tag{3.9}$$

To obtain the time derivative of a state in the interaction picture, let us differentiate Eq. 3.7 for the density matrix:

$$\frac{\partial}{\partial t}\rho^I(t) = \frac{i}{\hbar}[H_0,\rho^I] + e^{iH_0t/\hbar}\Big(\frac{\partial}{\partial t}\rho^S(t)\Big)e^{-iH_0t/\hbar} \tag{3.10}$$

and substitute from Eq. 3.9 (with the notation we introduced above):

$$\frac{\partial}{\partial t}\rho'(t) = \frac{i}{\hbar}[H_0,\rho'] + e^{iH_0t/\hbar}\Big(-\frac{i}{\hbar}[H_0+H_I,\rho]\Big)e^{-iH_0t/\hbar}. \tag{3.11}$$

Note now that $e^{iH_0t/\hbar}$ commutes with H_0 and that we are therefore left with

$$\frac{\partial}{\partial t}\rho'(t) = \frac{i}{\hbar}[H_0,\rho'] - \frac{i}{\hbar}[H_0,\rho'] + e^{iH_0t/\hbar}\Big(-\frac{i}{\hbar}[H_I,\rho]\Big)e^{-iH_0t/\hbar}, \tag{3.12}$$

which is equivalent to

$$\frac{\partial}{\partial t}\rho'(t) = -\frac{i}{\hbar}[H_I(t),\rho'(t)]. \tag{3.13}$$

This equation is the interaction picture form of the Liouville-von Neumann equation.

With this information, we are now equipped to derive the Redfield equation.

3.2 Derivation of the Redfield equation

The Redfield model is often used to describe the dynamics of a small quantum system that interacts significantly, but weakly, with a large number of other de-

grees of freedom. It provides an approximate, coarse-grained description of the relevant part of the system, while treating the large number of other degrees of freedom statistically.

For the derivation in this section, we will follow the approach of Refs. [65, 66].

In deriving the Redfield equation, we first integrate Eq. 3.13 formally to obtain

$$\rho'(t) = \rho'(0) - \frac{i}{\hbar}\int_0^t d\tau[H_I(\tau), \rho'(\tau)], \tag{3.14}$$

and again substitute this result back into the right hand side of Eq. 3.13:

$$\frac{\partial}{\partial t}\rho'(t) = -\frac{i}{\hbar}[H_I(t), \rho'(0)] - \frac{1}{\hbar^2}\int_0^t d\tau[H_I(t), [H_I(\tau), \rho'(\tau)]]. \tag{3.15}$$

We now take a trace over the bath degrees of freedom on both sides of Eq. 3.15. This amounts to averaging over these degrees of freedom. We are left with an expression for the reduced density matrix ρ_S that describes only the system degrees of freedom:

$$\frac{\partial}{\partial t}\rho'_S(t) = -\frac{i}{\hbar}\mathrm{tr}_B[H_I(t), \rho'(0)] - \frac{1}{\hbar^2}\int_0^t d\tau \mathrm{tr}_B[H_I(t), [H_I(\tau), \rho'(\tau)]]. \tag{3.16}$$

Up to now we have not made any approximations and Eq. 3.16 is therefore exact. This equation is not of much use, however, since the dynamics of the reduced density matrix still depends explicitly on the value of the full density matrix at previous times.

We can assume that the interaction is introduced at $t_0 = 0$ and that the full density matrix at t_0 can therefore be written as $\rho'(0) = \rho'_S(0)\rho'_B(0)$, where the tensor

UNIVERSITEIT VAN PRETORIA
UNIVERSITY OF PRETORIA
YUNIBESITHI YA PRETORIA

product is implied. Because we can choose t_0 to indicate the time at which the interaction starts, this is not really an approximation.

The first real approximation we introduce is the Born approximation. We assume that the bath consists of a vast number of degrees of freedom and that the state of the bath remains essentially unchanged by interaction with the system. If we assume that the bath was initially in thermal equilibrium, this equilibrium is maintained at all times. We can therefore substitute $\rho'(\tau)$ with $\rho'_S(\tau)\rho'_B(0)$ in Eq. 3.16:

$$\frac{\partial}{\partial t}\rho'_S(t) = -\frac{i}{\hbar}\mathrm{tr}_B[H_I(t),\rho'_S(0)\rho'_B(0)] - \frac{1}{\hbar^2}\int_0^t d\tau \mathrm{tr}_B[H_I(t),[H_I(\tau),\rho'_S(\tau)\rho'_B(0)]]. \tag{3.17}$$

We have now eliminated the complexity of the full density matrix from the dynamics of the reduced density matrix. The dynamics at time t still depends, however, on the dynamics at all prior times ($\rho'_S(t)$ depends on the $\rho'_S(\tau)$ in the integration kernel).

We also assume that the dissipative effect of the bath is so strong that the relevant system has a very short memory. This is known as the Markov approximation. In essence, the Markov approximation assumes that excitons equilibrate among the different vibrational levels rapidly (see Fig. 2.3) and that the relevant system can therefore not "deduce" its past from the occupancy of vibrational levels. Since the system at time t does not have a memory of itself at a prior time τ, we can replace $\rho'_S(\tau)$ with $\rho'_S(t)$ in the integration kernel:

$$\frac{\partial}{\partial t}\rho'_S(t) = -\frac{i}{\hbar}\mathrm{tr}_B[H_I(t),\rho'_S(0)\rho'_B(0)] - \frac{1}{\hbar^2}\int_0^t d\tau \mathrm{tr}_B[H_I(t),[H_I(\tau),\rho'_S(t)\rho'_B(0)]]. \tag{3.18}$$

We will also assume that the interaction Hamiltonian in the Schrödinger picture

has the form

$$H_I = \sum_i Q_i^S Q_i^B, \tag{3.19}$$

where Q_i^S and Q_i^B are system and bath operators respectively. In Section 3.4 we will show that the interaction Hamiltonian (for the model described in Chapter 2), indeed has this form.

In the interaction picture of H_0, Eq. 3.19 becomes:

$$\begin{aligned} H_I(t) &= \sum_i e^{iH_0 t} Q_i^S Q_i^B e^{-iH_0 t} \\ &= Q_i^S(t) Q_i^B(t). \end{aligned} \tag{3.20}$$

With this form of the interaction Hamiltonian, the first term of Eq. 3.18 equals

$$-\frac{i}{\hbar}\sum_i Q_i^S(t)\rho_S'(0)\mathrm{tr}_B(Q_i^B(t)\rho_B'(0)) + \frac{i}{\hbar}\sum_i \rho_S'(0)Q_i^S(t)\mathrm{tr}_B(Q_i^B(t)\rho_B'(0)), \tag{3.21}$$

where we used the facts that $Q_i^S(t)$ and $Q_j^B(t)$ commute, the trace operation acts only on the bath operators and the trace is invariant under rotation of its arguments.

We will show in Section 3.4 that the bath operators are simply nuclear coordinates (of which we can define the reference frames as we wish, of course). In particular, we define the bath operators in such a way that their equilibrium expectation values, $\mathrm{tr}_B(Q_i^B(t)\rho_B'(0))$, are zero. The first term in Eq. 3.18 then falls away.

Substituting Eq. 3.20 into Eq. 3.18 and expanding the commutators yields

$$\begin{aligned}\frac{\partial}{\partial t}\rho'_S(t) = -\frac{1}{\hbar^2}\sum_{i,j}\int_0^t d\tau \mathrm{tr}_B\big\{&Q_i^S(t)Q_j^S(\tau)Q_i^B(t)Q_j^B(\tau)\rho'_S(t)\rho'_B(0)\\ &-Q_j^S(\tau)Q_j^B(\tau)\rho'_S(t)\rho'_B(0)Q_i^S(t)Q_i^B(t)\\ &+\rho'_S(t)\rho'_B(0)Q_j^S(\tau)Q_i^S(t)Q_j^B(\tau)Q_i^B(t)\\ &-Q_i^S(t)Q_i^B(t)\rho'_S(t)\rho'_B(0)Q_j^S(\tau)Q_j^B(\tau)\big\}.\end{aligned} \tag{3.22}$$

Using the cyclic property of the trace and the fact that $Q_i^S(t)$ and $Q_j^B(t)$ commute, we obtain

$$\begin{aligned}\frac{\partial}{\partial t}\rho'_S(t) = -\frac{1}{\hbar^2}\sum_{i,j}\int_0^t d\tau \Big[&\big(Q_i^S(t)Q_j^S(\tau)\rho'_S(t) - Q_j^S(\tau)\rho'_S(t)Q_i^S(t)\big)\mathrm{tr}_B\big\{Q_i^B(t)Q_j^B(\tau)\rho'_B(0)\big\}\\ &+\big(\rho'_S(t)Q_j^S(\tau)Q_i^S(t) - Q_i^S(t)\rho'_S(t)Q_j^S(\tau)\big)\mathrm{tr}_B\big\{Q_j^B(\tau)Q_i^B(t)\rho'_B(0)\big\}\Big].\end{aligned} \tag{3.23}$$

The traces in Eq. 3.23 are two-times correlation functions

$$\mathrm{tr}_B\big\{Q_i^B(t)Q_j^B(\tau)\rho'_B(0)\big\} = \langle Q_i^B(t)Q_j^B(\tau)\rangle, \tag{3.24}$$

where $\langle\ldots\rangle$ indicates an expectation value (average).

We next assume that the correlation functions $\langle Q_j^B(\tau)Q_i^B(t)\rangle$ do not depend on the absolute time, but only on the time that passed since an excita-

UNIVERSITEIT VAN PRETORIA
UNIVERSITY OF PRETORIA
YUNIBESITHI YA PRETORIA

tion ($t' = t - \tau$). We also assume that the correlation functions $C_{ij}(t') = \langle Q_i^B(t) Q_j^B(\tau)\rangle = \langle Q_i^B(t') Q_j^B(0)\rangle$ decay exponentially, and very fast compared to the dynamics of the relevant system. We can therefore make the approximation that $C_{ij}(t')$ is nonzero only when t' is smaller than a critical time, t_R, called the correlation time of the bath.

Changing the variable of integration to t' (the limits do not change), Eq. 3.23 then becomes:

$$\frac{\partial}{\partial t}\rho_S'(t) = -\frac{1}{\hbar^2}\sum_{i,j}\int_0^t dt' \Big\{ \big(Q_i^S(t) Q_j^S(t-t')\rho_S'(t) - Q_j^S(t-t')\rho_S'(t) Q_i^S(t)\big)\langle Q_i^B(t') Q_j^B(0)\rangle + \big(\rho_S'(t) Q_j^S(t-t') Q_i^S(t) - Q_i^S(t)\rho_S'(t) Q_j^S(t-t')\big)\langle Q_i^B(0) Q_j^B(t')\rangle \Big\}. \tag{3.25}$$

We now assume that $t >> t_R$. This means that we calculate the relevant system dynamics over times that are much longer than the timescale of bath dynamics (this is why Redfield theory is called a *coarse-grained* description). Since $t >> t_R$, and the correlation functions are zero in this regime, the upper integration limit in Eq. 3.25 can be extended to infinity. The terms in the integrand can also be grouped together to form commutators:

$$\frac{\partial}{\partial t}\rho_S'(t) = -\frac{1}{\hbar^2}\sum_{i,j}\int_0^\infty dt' \Big\{ [Q_i^S(t), Q_j^S(t-t')\rho_S'(t)] C_{ij}(t') + [\rho_S'(t) Q_j^S(t-t'), Q_i^S(t)] C_{ij}(-t') \Big\}. \tag{3.26}$$

We now transform Eq. 3.26 to the Schrödinger picture by using the Heisenberg equation (Eq. 3.8):

$$\frac{\partial}{\partial t}\rho_S(t) = -\frac{i}{\hbar}[H_{RS},\rho_S(t)] - \frac{1}{\hbar^2}\sum_{i,j}\int_0^\infty dt' e^{-iH_0 t/\hbar}\Big\{[Q_i^S(t),Q_j^S(t-t')\rho_S'(t)]C_{ij}(t') + [\rho_S'(t)Q_j^S(t-t'),Q_i^S(t)]\Big\}e^{iH_0 t/\hbar}C_{ij}(-t'), \tag{3.27}$$

where we used $[H_0,\rho_S(t)] = [H_{RS},\rho_S(t)]$, since H_B and ρ_S commute.

The last steps now are to express this equation in the eigenbasis of the relevant system Hamiltonian and simplify the result. To this end, suppose that $|\alpha\rangle$ and $|\beta\rangle$ are eigenvectors of this basis with eigenvalues α and β. It therefore holds that $\langle\alpha|e^{-iH_0 t/\hbar} = \langle\alpha|e^{-i\alpha t/\hbar}\cdot e^{-iH_B t/\hbar}$, since H_{RS} and H_B commute. In the eigenbasis representation Eq. 3.27 therefore becomes

$$\langle\alpha|\frac{\partial}{\partial t}\rho_S(t)|\beta\rangle = -\frac{i}{\hbar}\langle\alpha|[H_{RS},\rho_S(t)]|\beta\rangle - \frac{1}{\hbar^2}\sum_{i,j}\int_0^\infty dt'\Big\{\langle\alpha|e^{-i\alpha t/\hbar}[Q_i^S(t),Q_j^S(t-t')\rho_S'(t)]e^{i\beta t/\hbar}|\beta\rangle C_{ij}(t') + \langle\alpha|e^{-i\alpha t/\hbar}[\rho_S'(t)Q_j^S(t-t'),Q_i^S(t)]e^{i\beta t/\hbar}|\beta\rangle C_{ij}(-t')\Big\}. \tag{3.28}$$

Now, notice that

$$-\frac{i}{\hbar}\langle\alpha|[H_{RS},\rho_S(t)]|\beta\rangle = -\frac{i}{\hbar}\langle\alpha|(\alpha-\beta)\rho_S(t)|\beta\rangle \tag{3.29}$$

and

$$\begin{aligned}\langle\alpha|\, e^{-i\alpha t/\hbar}[Q_i^S(t), Q_j^S(t-t')\rho_S'(t)]e^{i\beta t/\hbar}\,|\beta\rangle \\ = \langle\alpha|\left(Q_i^S e^{-iH_{RS}t'/\hbar}Q_j^S e^{+iH_{RS}t'/\hbar}\rho_S\right. \\ \left. - e^{-i\alpha t'/\hbar}Q_j^S e^{iH_{RS}t'/\hbar}\rho_S Q_i^S\right)|\beta\rangle\,.\end{aligned} \tag{3.30}$$

We can multiply with identities $\sum_\gamma |\gamma\rangle\langle\gamma|$ (where the summation is over the entire eigenbasis) throughout to obtain

$$\begin{aligned}&\langle\alpha|\left(Q_i^S e^{-iH_{RS}t'/\hbar}\sum_\gamma |\gamma\rangle\langle\gamma| Q_j^S e^{iH_{RS}t'/\hbar}\sum_\delta |\delta\rangle\langle\delta|\rho_S\right. \\ &\left. - e^{-i\beta t'/\hbar}Q_j^S e^{iH_{RS}t'/\hbar}\sum_\nu |\nu\rangle\langle\nu|\rho_S\sum_\mu |\mu\rangle\langle\mu| Q_i^S\right)|\beta\rangle \\ &= \sum_\gamma\sum_\delta \langle\alpha| Q_i^S|\gamma\rangle\langle\gamma| Q_j^S|\delta\rangle\langle\delta|\rho_S|\beta\rangle\, e^{i(\delta-\gamma)t'/\hbar} \\ &- \sum_\gamma\sum_\delta \langle\alpha| Q_j^S|\delta\rangle\langle\delta|\rho_S|\gamma\rangle\langle\gamma| Q_i^S|\beta\rangle\, e^{i(\delta-\alpha)t'/\hbar}.\end{aligned} \tag{3.31}$$

Similarly, for the second commutator in Eq. 3.28 we obtain

$$\begin{aligned}&\langle\alpha|\, e^{-i\alpha t/\hbar}[\rho_S'(t)Q_j^S(t-t'), Q_i^S(t)]e^{i\beta t/\hbar}\,|\beta\rangle \\ &= \sum_\gamma\sum_\delta \langle\alpha|\rho_S|\gamma\rangle\langle\gamma| Q_j^S|\delta\rangle\langle\delta| Q_i^S|\beta\rangle\, e^{i(\delta-\gamma)t'/\hbar} \\ &- \sum_\gamma\sum_\delta \langle\alpha| Q_i^S|\delta\rangle\langle\delta|\rho_S|\gamma\rangle\langle\gamma| Q_j^S|\beta\rangle\, e^{i(\beta-\gamma)t'/\hbar}.\end{aligned} \tag{3.32}$$

With these expressions, we obtain the Redfield relaxation equation

$$\frac{\partial}{\partial t}\rho_{\alpha\beta}(t) = -\frac{i}{\hbar}\omega_{\alpha\beta}\rho_{\alpha\beta}(t) - \sum_{\delta,\gamma} R_{\alpha\beta\gamma\delta}\rho_{\gamma\delta}(t), \tag{3.33}$$

where

$$\omega_{\alpha\beta} = \alpha - \beta \tag{3.34}$$

and

$$\begin{aligned} R_{\alpha\beta\gamma\delta} = -\frac{1}{\hbar^2}\int_0^\infty dt' \{ &\Lambda_{\delta\beta\alpha\gamma} e^{-i\omega_{\delta\beta}t'} + \Lambda_{\delta\beta\alpha\gamma} e^{-i\omega_{\alpha\gamma}t'} \\ &- \delta_{\delta\beta}\sum_s \Lambda_{\alpha ss\gamma} e^{-i\omega_{s\gamma}t'} - \delta_{\gamma\alpha}\sum_s \Lambda_{\delta ss\beta} e^{-i\omega_{\delta s}t'} \}, \end{aligned} \tag{3.35}$$

with

$$\Lambda_{\delta\beta\alpha\gamma} = \sum_i \sum_j \langle\alpha| Q_j^S |\delta\rangle \langle\gamma| Q_i^S |\beta\rangle C_{ij}(t'), \tag{3.36}$$

and $\delta_{\alpha\beta}$ the Kronecker delta.

Eq. 3.33 describes the dynamics of the reduced density matrix because of relaxation by the environment. The Redfield relaxation tensor, Eq. 3.35, determines the rate of transfer between populations (for R_{aabb}), between populations and coherences (R_{aabc} and R_{bcaa}) and between coherences (R_{abcd} and R_{abab}). One further approximation brings us to the secular Redfield equation which we will use in the next chapters.

3.3 Secular approximation

The following explanation of the secular approximation is given by Olšina and Mančal [67].

UNIVERSITEIT VAN PRETORIA
UNIVERSITY OF PRETORIA
YUNIBESITHI YA PRETORIA

In the interaction picture, the Redfield equation (Eq. 3.33) is

$$\frac{\partial}{\partial t}\rho'_{\alpha\beta}(t) = -\sum_{\gamma,\delta} R_{\alpha\beta\gamma\delta}\rho'_{\gamma\delta}(t)e^{i(\omega_{\gamma\delta}-\omega_{\alpha\beta})t/\hbar}. \tag{3.37}$$

To solve this equation, we integrate on both sides of the equality. The exponential $e^{i(\omega_{\gamma\delta}-\omega_{\alpha\beta})t/\hbar}$ will then cause the integrand on the right-hand side to oscillate if $\omega_{\gamma\delta}-\omega_{\alpha\beta} \neq 0$. If the energy difference between different exciton states are large enough for the factors $e^{i(\omega_{\gamma\delta}-\omega_{\alpha\beta})}$ to vary much faster than the factor $R_{\alpha\beta\gamma\delta}\rho'_{\gamma\delta}(t)$, one expects all terms for which $\omega_{\gamma\delta}-\omega_{\alpha\beta} \neq 0$ to oscillate so fast that their integrals average to zero. We make this approximation explicit by setting all $R_{\alpha\beta\gamma\delta}$ equal to zero except those for which $\alpha = \gamma$ and $\alpha = \delta$ or in which $\alpha = \beta$ and $\gamma = \delta$. In the secular approximation regime, we do not allow transfer between populations and coherences or between different coherences ($R_{\alpha\beta\gamma\delta}$ where at least two of $\alpha, \beta, \gamma, \delta$ are unique).

3.4 Application to photosynthetic light harvesting

In many photosynthetic light-harvesting complexes, the coupling between pigment molecules is strong enough compared to the pigment-environment coupling, that the Redfield equation can be used to calculate the excitation dynamics. In principle, we can solve the set of coupled differential equations given by Eq. 3.33 if we have the initial state of the light-harvesting complex. In practice, this is done by calculating $\frac{\partial}{\partial t}\rho_{\alpha\beta}(t)$ for short sequential time steps and multiplying the time derivative for each time step by the corresponding density matrix element at the start of the interval. This method is explained in more detail in Chapter 5.

All of the variables and operators appearing in the Redfield equation, except two, have been discussed in the previous sections. In Eq. 3.19, we introduced the

interaction Hamiltonian in the form

$$H_I = \sum_i Q_i^S Q_i^B. \tag{3.38}$$

For the sake of keeping the derivation in Section 3.2 general, we did not explain the operators Q_i^S and Q_j^B. We will do so now.

In Section 2.4, we showed that the interaction Hamiltonian for the light-harvesting systems is given by

$$H_I = \sum_{i=1}^{N} \sum_k \hbar \omega_{ki} q_{ki} d_{ki} \left|e_i\right\rangle \left\langle e_i\right|. \tag{3.39}$$

Comparing this equation with Eq. 3.38, it is clear that

$$Q_i^S = \left|e_i\right\rangle \left\langle e_i\right| \qquad \text{and} \qquad Q_i^B = \sum_k \hbar \omega_{ki} d_{ki} q_{ki}. \tag{3.40}$$

The factors $\left\langle \alpha\right| Q_i^S \left|\delta\right\rangle$ are therefore simply

$$\left\langle \alpha\right| Q_j^S \left|\delta\right\rangle = \left\langle \alpha \right| e_i\left\rangle \right\langle e_i \left| \delta\right\rangle \tag{3.41}$$

and the correlation functions $\langle Q_i^B(t') Q_j^B(0)\rangle$ are

$$\langle Q_i^B(t') Q_j^B(0)\rangle = \langle \sum_k \hbar \omega_{ki} d_{ki} q_{ki}(t') \sum_l \hbar \omega_{lj} d_{lj} q_{lj}(0)\rangle. \tag{3.42}$$

3.5 Simplification of bath correlation functions

In the bath model discussed in Chapter 2, each electronic degree of freedom was coupled to a large number of independent harmonic oscillators. This model is

UNIVERSITEIT VAN PRETORIA
UNIVERSITY OF PRETORIA
YUNIBESITHI YA PRETORIA

often called the spin-boson model (i.e., a two-level system coupled to a bosonic bath).

An equivalent way of thinking about the spin-boson model is the so-called multimode Brownian oscillator model (MBO) [59]. In this model, the relevant system is linearly coupled to a finite set of harmonic oscillators. In turn, these harmonic oscillators (which we call the primary oscillators) are coupled linearly to a large (or infinite) number of other harmonic oscillators (which we call the free oscillators, since they are not coupled to the relevant system). A schematic of this model is shown in Fig. 3.1.

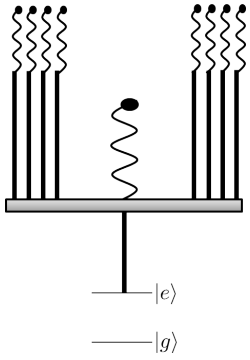

Figure 3.1: A schematic of the quantum multimode Brownian oscillator model. The straight vertical lines indicate linear coupling and the grey bar represents the primary oscillator mass. Oscillators are represented by springs. The secondary oscillators are allowed to have different frequencies and masses.

Notice that the bath coordinates enter the derivation of the Redfield equation through commutators of the relevant system-bath interaction Hamiltonian (see Eq. 3.18). Since the free oscillator coordinates are not coupled directly to the electronic degrees of freedom, the only correlation functions in the Redfield equation of a system with an MBO bath, are therefore the ones containing the coordinates of the primary oscillators.

Now suppose that, for each pigment molecule, the excited state is coupled to a single primary oscillator (because the spin-boson model is equivalent to the multimode Brownian oscillator model, such a choice is always permitted). It is often assumed in literature that excitations couple independently, with the same coup-

UNIVERSITEIT VAN PRETORIA
UNIVERSITY OF PRETORIA
YUNIBESITHI YA PRETORIA

ling constants, to identical baths. The correlation function above then becomes

$$\langle Q_i^B(t')Q_j^B(0)\rangle = \hbar^2\omega^2 d^2\langle q_i(t')q_j(0)\rangle, \tag{3.43}$$

where q_i is the coordinate of the primary oscillator that couples directly to excitation on site i, ω is the angular frequency and d the coupling parameter for this oscillator (see Section 2.4).

The primary oscillator is the link between the free bath and the relevant system, and the effect of these two subsystems on each other should therefore be channelled through the primary oscillator. All the dynamics of the bath that have an influence on the system can be therefore be obtained by a characterisation of the primary oscillator coordinate. The bath correlation functions provide such a characterisation. The exact form of the correlation function depends on the spectral density of the bath. Later, we will use the correlation function of an overdamped Brownian oscillator (as explained in Chapter 5).

UNIVERSITEIT VAN PRETORIA
UNIVERSITY OF PRETORIA
YUNIBESITHI YA PRETORIA

Chapter 4

Multiexcitonic systems

In the previous chapters, we considered the case of a single excitation in a light-harvesting system. Under natural conditions, however, light intensity is often strong enough for more than one excitation to be present simultaneously [49, 68]. As noted by Abramavicius et al. [68], interactions of these excitons cause dissipation of energy through singlet-singlet or singlet-triplet annihilation (see Refs. [57,69] for discussions of annihilation). As also noted by Abramavicius et al. [68], consideration of multiple-exciton interactions are important for the description of coherent control of excited state dynamics in photosynthetic light harvesting [70]. In addition, simulation of nonlinear optical spectroscopy experiments (like fluorescence depolarisation, hole-burning, pump-probe etc.) requires a theory that takes into account the interactions of multiple excitons [71]. Knowing the initial multiple-exciton dynamics (i.e., before the interactions occur) in light-harvesting systems is important to determine where, and how frequently, interactions occur. Developing a formalism for calculating such dynamics will be the focus of this chapter.

For the sake of simplicity, we will consider only the case where two excitations

are simultaneously present, but all the ideas that are developed here can easily be extrapolated to systems containing more than two excitations.

4.1 Two-exciton Hamiltonians

Suppose that pigment molecules i and j are excited. We denote this compound state by $|e_I\rangle = |e_i e_j\rangle = |e_j e_i\rangle$, where i and j are never equal and pair (i, j) is unique for each value of I. To account for these double-excitation states, we should add to the system Hamiltonian (Eq. 2.3) their excitation energies and couplings:

$$\sum_{I=1}^{N(N-1)/2} E_{e_I} |e_I\rangle \langle e_I| \quad \text{and} \quad \sum_{I\neq J}^{N(N-1)/2} V_{IJ} |e_I\rangle \langle e_J| , \tag{4.1}$$

where E_{e_I} is the excitation energy of state I and V_{IJ} is the coupling between states I and J. Notice that there are $\frac{N(N-1)}{2}$ unique ways to excite two sites in a molecular aggregate with N sites.

The two-excitation energies and couplings can easily be expressed in terms of their single-excitation counterparts. To do this, notice first that the reorganisation term $\sum_k \frac{\hbar\omega_{ki}}{2} d_{ki}^2$ in Eq. 2.5 forms part of the energy needed to excite a pigment molecule in an aggregate. As is often done in literature [72], we will assume that each excitation in a two-excitation state couples independently to the bath. This means that the excitation energies of the two pigment molecules in a two-excitation state are also independent. The energy of the two-excitation state $|e_I\rangle = |e_i e_j\rangle$ is therefore simply

$$\varepsilon_I = \varepsilon_i + \varepsilon_j. \tag{4.2}$$

The coupling between two-excitation states can also be obtained from the single-excitation couplings: Notice that independent coupling of pigment molecules to

the bath means that the interpigment coupling is not affected by the creation of a two-excitation state. For $I = (i, j)$ and $J = (k, l)$ we therefore have that

$$V_{IJ} = \frac{1}{2}\left[\delta_{ik}V_{jl} + \delta_{jk}V_{il} + \delta_{il}V_{jk} + \delta_{jl}V_{ik}\right], \tag{4.3}$$

where the factor $\frac{1}{2}$ compensates for double-counting (because $V_{jl} = V_{lj}$).

The bath Hamiltonian remains the same as in the single-excitation case. Because pigment molecules couple independently to the bath, the two-exciton contribution to the interaction Hamiltonian is simply

$$H_I^{\text{2-ex}} = \sum_{I=1}^{N(N-1)/2} \sum_K \hbar\omega_{KI} q_{KI} d_{KI} \left|e_I\right\rangle \left\langle e_I\right|, \tag{4.4}$$

where

$$\hbar\omega_{KI} q_{KI} d_{KI} = \hbar\omega_{ki} q_{ki} d_{ki} + \hbar\omega_{kj} q_{kj} d_{kj} \qquad \text{if } I = (i, j). \tag{4.5}$$

4.2 Bases for describing excitation dynamics

In Section 2.6, we described the site basis and exciton basis for single-excitation systems. Extension of the bases to multi-excitation systems is straightforward.

Site basis

The site basis of a two-excitation system is the set of states $\{\left|e_I\right\rangle = \left|e_i e_j\right\rangle = \left|e_j e_i\right\rangle \;\; | \;\; i \neq j\}$, where the system is in state $\left|e_I\right\rangle$ if the i^{th} and j^{th} pigment molecules are excited and all other pigment molecules are in their ground states. Just like in the single-excitation case, the site basis for a two-excitation system is orthonormal (i.e., $\left\langle e_I \middle| e_J\right\rangle = \delta_{IJ}$). It is important to notice that the total site-basis

UNIVERSITEIT VAN PRETORIA
UNIVERSITY OF PRETORIA
YUNIBESITHI YA PRETORIA

population of a two-excitation system is one, but that the populations of individual sites add to two (since there are two excitations).

Eigenbasis

As was the case for the single-excitation eigenbasis, the two-excitation eigenbasis is formed from a set of orthonormal eigenvectors of the two-excitation Hamiltonian. Such vectors can, again, be found from the columns of the matrix that diagonalise the two-excitation Hamiltonian.

4.3 Dynamics of multiexcitonic systems

Almost all of the concepts in Chapter 2 can be extended directly to multiexcitonic systems. The only difference is that the Hamiltonian eigenstates are now two-exciton states. The mechanism through which the bath relaxes the relevant system remains exactly the same: The two-exciton states couple linearly to the bath. This interaction causes irreversible relaxation of the two-exciton states until their energies are described by the Boltzmann distribution.

The Redfield equation was derived in Chapter 3 without ever specifying the number of excitations in the system, and is therefore valid for systems with any number of excitations (as long as the coupling between pigment molecules in such a system is much stronger than coupling to the bath). The two-exciton Redfield dynamics is therefore calculated in the same way as single-exciton Redfield dynamics, except that we now use the two-exciton basis states and two-exciton correlation functions.

For calculating the single-exciton Redfield dynamics, we used the correlation

UNIVERSITEIT VAN PRETORIA
UNIVERSITY OF PRETORIA
YUNIBESITHI YA PRETORIA

functions (see Sections 3.4 and 3.5):

$$\langle Q_i^B(t')Q_j^B(0)\rangle = \hbar^2\omega^2 d^2 \langle q_i(t')q_j(0)\rangle. \tag{4.6}$$

The two-excitation correlation functions can easily be found from the single-excitation correlation functions:

$$\langle q_I(t')q_J(0)\rangle = \langle \big(q_i(t') + q_j(t')\big) \cdot \big(q_k(0) + q_l(0)\big)\rangle, \tag{4.7}$$

where $I = (i, j)$ and $J = (k, l)$.

Since the bath coordinates at different sites are uncorrelated (see Section 4.1), $\langle q_I(t')q_J(0)\rangle$ equals zero if the sites constituting I and J are all unique, and it is equal to $\big(\langle q_i(t')q_i(0)\rangle + \langle q_j(t')q_j(0)\rangle\big)$ if $I = J = (i, j)$. If only site i is shared between I and J, then $\langle q_I(t')q_J(0)\rangle = \langle q_i(t')q_i(0)\rangle$.

4.4 Towards a single-exciton description of a multiexcitonic system

Calculating the exciton dynamics of a system becomes drastically more tedious when the number of excitons increases. For a system with N sites and $n \leqslant N$ excitons, one has to calculate the dynamics of $\big(\frac{(N!)}{(N-n)!n!}\big)^2$ density matrix elements! This quantity (as a function of number of excitons, n) is shown in Fig. 4.1 for four natural light-harvesting complexes: FMO, an excitation conduit in green sulphur bacteria, containing eight bacteriochlorophylls; LH1 and LH2, bacterial light-harvesting complexes containing 32 and 27 bacteriochlorophylls, respectively; and LHCII, the main light-harvesting complex in plants, containing 14 chlorophylls.

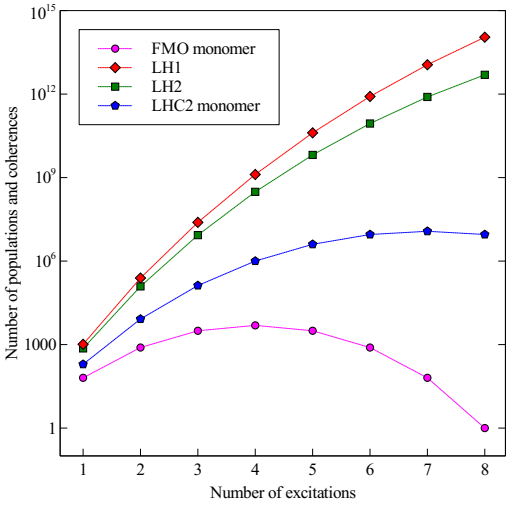

Figure 4.1: The number of density matrix elements as a function of number of excitations for the FMO monomer (8 pigments), LHCII monomer (14 pigments), LH2 (27 pigments), LH1 (32 pigments).

It is clear that even the calculation of *two*-exciton dynamics in some light-harvesting complexes (like LH1 and LH2) is computationally arduous.

Based on phenomenological reasoning, it is reasonable to expect that, for the case of two completely localised excitons (i.e., for a system in the Förster limit), the populations of individual sites are described by the equation

$$\frac{d}{dt}P_i = \sum_{l\neq i} P_l(1-P_i)R_{il} - P_i\sum_{l\neq i}(1-P_l)R_{li}, \tag{4.8}$$

where R_{il} is the single-exciton transfer rate from site l to site i.

The terms $(1-P_i)$ would then prevent double excitation of site i: if i were occupied fully, no population would be transferred to this site.

If Eq. 4.8 were correct, computation of multi-excitation Förster dynamics would be significantly simplified! Furthermore, similarities between Förster-type and Redfield-type dynamics[1] could mean that a similar equation exists to determine multiexcitonic Redfield-type dynamics. This would reduce the number of density matrix elements from $\left(\frac{(N!)}{(N-n)!n!}\right)^2$ to N; a significant improvement!

[1] In both cases, no individual site is allowed to have a population of more than one.

At the start of the research leading to this dissertation, we compared the results of a simulation based on Eq. 4.8 and a simulation based on the full two-exciton master equation

$$\frac{d}{dt}P_{ij} = -P_{ij}\Big(\sum_{l}\sum_{m} R_{lm\leftarrow ij}\Big) + \Big(\sum_{l}\sum_{m} P_{lm}R_{ij\leftarrow lm}\Big). \tag{4.9}$$

These two equations appeared to yield identical dynamics, and we assumed, therefore, that Eq. 4.8 was correct. We could also derive Eq. 4.8 analytically if we made the assumption that $P_{ab} = P_a P_b$ (see Appendix B). Notwithstanding much effort, we were unable to validate this assumption...

A year later, we tested Eq. 4.8 again and showed that this equation, in fact, produces only approximately correct dynamics at finite temperatures. We realised then that we tested only a special case of this equation initially—the case of infinite temperature when the rates R_{ij} and R_{ji} are equal. In reality, the forward and backward rates are not equal, but their ratio is given by the Boltzmann factor as explained in Section 2.5. The discrepancy between dynamics predicted by Eq. 4.8 and Eq. 4.9 proves that the assumption $P_{ab} = P_a P_b$ in Appendix B is invalid. In retrospect, the invalidity of this assumption should have been anticipated: only for two particles diffusing freely, would the probability of simultaneous occupation of sites a and b at time t be the product of probabilities of having site a excited at t, and having site b excited at t.

The analogy between Redfield-type energy transfer and Förster-type transfer is also not as strong as we initially believed. In the Redfield case, any two-exciton state can be written as a linear combination of direct products of single-exciton states, $\sum_{a,b} c_{ab}\,|a\rangle\,|b\rangle$. Terms such as $|a\rangle\,|a\rangle$ are also allowed in such an expansion [68]. In the Redfield case, single-exciton states are therefore allowed to have populations greater than one (as long as no pigment molecule has a population

UNIVERSITEIT VAN PRETORIA
UNIVERSITY OF PRETORIA
YUNIBESITHI YA PRETORIA

greater than one).

We cannot exclude the possibility for two-exciton dynamics to be expressed as the dynamics of single-exciton states, but from the discussion above, such a description will probably differ significantly from the form of Eq. 4.8.

UNIVERSITEIT VAN PRETORIA
UNIVERSITY OF PRETORIA
YUNIBESITHI YA PRETORIA

Chapter 5

Simulation

We wrote a computer program that calculates the Redfield-dynamics of single-exciton and two-exciton systems. This program was written in the GNU Octave language (for more detail about this language, see Ref. [73]). In this chapter we discuss the workings of this program.

5.1 Inputs

The program requires the following inputs: temperature, average reorganisation energy and average correlation time of the bath, the electronic Hamiltonian[1], and an initial density matrix. For calculating two-exciton dynamics, the program requires the initial density matrix in two-excitation site basis or two-excitation exciton basis, but still requires the electronic Hamiltonian in single-excitation site basis[2]. From this single-excitation site-basis Hamiltonian, the program cal-

[1] The Hamiltonian that has the form of Eq. 2.5 (i.e., with the reorganisation energy included).

[2] This is the natural basis for the Hamiltonian since the coupling between pigment molecules can be calculated from structural studies [74]. Attempts are also made at calculating site energies from structural data (see, for example, ref. [75]).

UNIVERSITEIT VAN PRETORIA
UNIVERSITY OF PRETORIA
YUNIBESITHI YA PRETORIA

culates the single-excitation exciton-basis Hamiltonian, two-excitation site-basis Hamiltonian and two-excitation exciton-basis Hamiltonian.

5.2 Algorithm and output

Single-exciton dynamics

The site-basis electronic Hamiltonian is first diagonalised. The eigenstates and eigenvalues obtained from the diagonalisation procedure, which comes predefined with Octave, are the exciton states and exciton energies, respectively. The difference between the diagonal elements in the exciton-basis Hamiltonian are the ω's in Eq. 3.33. The same unitary transformation that was used for the diagonalisation of the electronic Hamiltonian is also used to transform the initial density matrix to the exciton basis.

The evolution of the exciton-basis density matrix over a time t is performed by first calculating the Redfield tensor, Eq. 3.35, for a finite set of points in time $\{t_i | i \geqslant 1\}$ such that $t_i < t_{i+1}$ and $\forall\, i \;:\; t_{i+1} - t_i = dt$. The Redfield tensor $R_{\alpha\beta\delta\gamma}(t_i)$ is calculated by substituting the correlation function $C_{ij}(t_i)$ into Eq. 3.35. We used the overdamped harmonic oscillator correlation function for this program [67]. This correlation function is often used in simulations, because it can be calculated analytically and depends on only three physical parameters: the temperature, bath correlation time and the bath reorganisation energy.

The next step in calculating the evolution is to separate the populations and coherences from the initial exciton-basis density matrix. The separate evolution is allowed because of the secular approximation (see Section 3.3). The populations

and coherences are then evolved over t by the Redfield equation

$$\frac{\partial}{\partial t}\rho_{\alpha\beta}(t_{i+1}) = -\frac{i}{\hbar}\omega_{\alpha\beta}\rho_{\alpha\beta}(t_i) - \sum_{\gamma,\delta} R_{\alpha\beta\gamma\delta}(t_{i+1})\rho_{\gamma\delta}(t_i). \tag{5.1}$$

After each iteration of Eq. 5.1, the populations and coherences are stored. If the site basis was chosen as the output basis, the populations and coherences are recombined into a density matrix, which is transformed to the site basis and dismantled into populations and coherences again for storage.

Two-exciton dynamics

The two-exciton dynamics are expressed in the two-exciton site basis or two-exciton eigenbasis (see Section 4.2). The algorithm for calculating two-exciton dynamics is the same as described above for the single-exciton case. The two-excitation Hamiltonian is calculated, however, as described in Section 4.1. The two-excitation correlation functions are obtained from the single-excitation correlation functions as described in Section 4.3.

UNIVERSITEIT VAN PRETORIA
UNIVERSITY OF PRETORIA
YUNIBESITHI YA PRETORIA

Chapter 6

Dynamics in molecular aggregates (examples)

In this chapter, we demonstrate the calculation of Redfield dynamics in three example systems. We first consider a very simple system: a six-chromophore ring. This provides a clear illustration of how the single-excitation and two-excitation site-basis Hamiltonians are assembled, their exciton states and exciton energy levels found and their excitation dynamics interpreted. We then calculate the Redfield dynamics for two photosynthetic complexes (FMO and LHCII) and compare these dynamics with published results.

6.1 Six-pigment ring with nearest neighbour coupling

6.1.1 Exciton states and exciton energies

Consider a ring of six pigment molecules in which only nearest neighbours are coupled and the coupling is identical for all neighbouring pairs (Fig. 6.1).

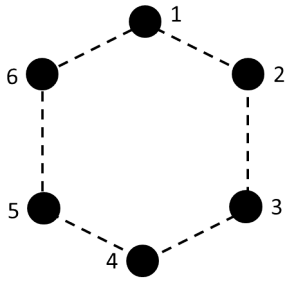

Figure 6.1: Six-chromophore ring with equal nearest neighbour coupling.

The site-basis Hamiltonian for the ring is

$$H = \begin{bmatrix} 1 & 0.1 & 0 & 0 & 0 & 0.1 \\ 0.1 & 1 & 0.1 & 0 & 0 & 0 \\ 0 & 0.1 & 1 & 0.1 & 0 & 0 \\ 0 & 0 & 0.1 & 1 & 0.1 & 0 \\ 0 & 0 & 0 & 0.1 & 1 & 0.1 \\ 0.1 & 0 & 0 & 0 & 0.1 & 1 \end{bmatrix}, \tag{6.1}$$

where the diagonal elements are the site energies (in the same order as the pigment numbers in Fig. 6.1) and the off-diagonal elements are the coupling strengths between sites (a strength of 0.1 was chosen arbitrarily).

The eigenvalues (exciton energies) and corresponding eigenvectors of this Hamiltonian can be found computationally by a diagonalisation procedure. The

first matrix below contains the eigenvalues and the second matrix the corresponding eigenvectors as columns.

$$\begin{bmatrix} 3 \\ 2 \\ 2 \\ -1 \\ 0 \\ 0 \end{bmatrix}, \begin{bmatrix} 1 & 1 & -1 & -1 & -1 & -1 \\ 1 & 0 & -1 & 1 & 0 & 1 \\ 1 & -1 & 0 & -1 & 1 & 0 \\ 1 & -1 & 1 & 1 & -1 & -1 \\ 1 & 0 & 1 & -1 & 0 & 1 \\ 1 & 1 & 0 & 1 & 1 & 0 \end{bmatrix}. \tag{6.2}$$

The exciton state with the lowest energy (-1) is therefore $\frac{1}{\sqrt{6}}\big(-|1\rangle+|2\rangle-|3\rangle+|4\rangle-|5\rangle+|6\rangle\big)$.

Since the six pigment molecules have the same site energies, the degeneracy in two of the exciton energy levels is not surprising. It is also reasonable to expect all pigment molecules to contribute equally to any equilibrium state of the system. This equal contribution is reflected directly in the first and fourth eigenvectors, where the magnitudes of each eigenvector's elements are equal. The second and third eigenvectors have the same energies and any vector in their span is therefore an eigenvector of the Hamiltonian (Eq. 6.1). Since all these eigenstates have the same energy, they have the same probability of being realised in an ensemble of systems. Even though the sites do not contribute equally to these eigenvectors, the ensemble average of these vectors corresponds to equal contribution by all sites. The same argument holds for the last two eigenvectors in Eq. 6.2.

To compose the two-excitation site-basis Hamiltonian, we first need to enumerate the two-excitation site-basis states (see Section 4.2). Let's choose (1,2) to be state 1, (1,3) to be state 2, (1,4) as state 3 etc. From Section 4.1, we know that the

UNIVERSITEIT VAN PRETORIA
UNIVERSITY OF PRETORIA
YUNIBESITHI YA PRETORIA

energy of state 1 is $\varepsilon_1 + \varepsilon_2$, where ε_1 is the site energy of chromophore 1. We also know from Section 4.1 that the coupling between the two-excitation site-basis states 1 and 2 is V_{23}, the single-exciton coupling between pigment molecules 2 and 3. The two-excitation Hamiltonian for this system therefore has the form

$$H = \begin{bmatrix} 2 & 0.1 & 0 & \dots \\ 0.1 & 2 & 0.1 & \dots \\ 0 & 0.1 & 2 & \dots \\ \vdots & \vdots & \vdots & \ddots \end{bmatrix}. \tag{6.3}$$

The exciton states and exciton energies are found in the same way as we did in the single-exciton case.

6.1.2 Exciton dynamics

The exciton dynamics of the six-member ring were calculated from an initial state in which the populations of sites 1, 2, 3 and 4 were 0.3, 0.3, 0.2 and 0.2, respectively, and there was no coherence between any sites. This initial state was chosen arbitrarily, but the essential properties of excitation dynamics is captured by the evolution of the system from this initial state. These dynamics are shown in Fig. 6.2.

The site-basis Hamiltonian (Eq. 6.1) is not diagonal. Initial exciton-basis populations (Fig. 6.2**a**) are therefore different from the site-basis populations (Fig. 6.2**b**). The site-basis states are linear combinations of the exciton states and the initial density matrix in exciton basis therefore contains non-zero coherences (Fig. 6.2**c**). The exciton states relax to the Boltzmann distribution with rates determined by the Redfield equation. In the equilibrium state of the system, all the sites contribute equally (Fig. 6.2**b**). This confirms the observation we made earlier that,

UNIVERSITEIT VAN PRETORIA
UNIVERSITY OF PRETORIA
YUNIBESITHI YA PRETORIA

even for non-symmetric states, pigments contribute equally at equilibrium. When the system is in equilibrium, pure (exciton) states are populated. The loss of coherence between exciton states in Fig. 6.2**c** is therefore not surprising. Fig. 6.2**d** depicts the coherences between site-basis states. The coherences between these states were chosen to be zero initially. Coherences between the sites are then induced until the linear combinations that produce these coherences are equal to the exciton states.

Oscillations in the real parts of coherences between excitons (shown in Fig. 6.2**c**) is of little physical significance. They arise simply from complex rotation by the non-interaction part of the full Hamiltonian (i.e., H_0 in the partitioning of Section 3.1.2). In the absence of relevant system-bath coupling, this rotation would have caused unitary time evolution.

Oscillations in the site-basis populations arise because of the transfer of excitation between exciton states. An easy way of understanding this occurrence is by considering three imaginary exciton states: state 1 having a high contribution from site j, state 2 having a low contribution from j and state 3, again having a high contribution from j. If population flows along the pigment molecule pathway $1 \rightarrow 2 \rightarrow 3$, oscillation of population j would be observed. In a regular system, such as our six-pigment ring, where excitation is delocalised over the whole structure, significant oscillation is not surprising. When such oscillations are observed, one can think of the excitation as a wave pulse travelling through the system.

The oscillations in Fig. 6.2**d** is due to the complex evolution by the non-interaction Hamiltonian, as well as the wavelike transfer of energy discussed above.

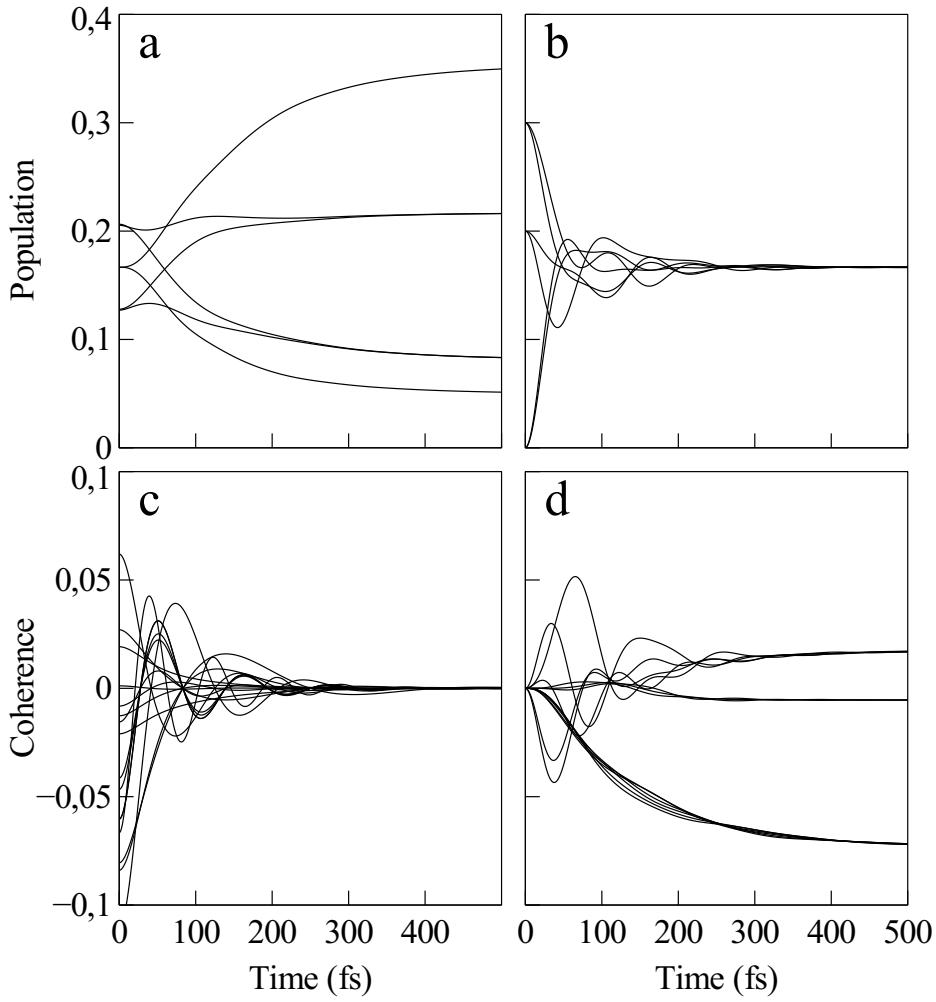

Figure 6.2: The excitation dynamics in a six-member ring of pigment molecules. **a** The exciton-basis populations, **b** site-basis population, **c** exciton-basis coherences (real parts), **d** site-basis coherences (real parts).

6.2 Fenna-Matthews-Olson complex

The Fenna-Matthews-Olson (FMO) complex is a pigment-protein complex found in green sulphur bacteria [76]. Many species of these bacteria live in extremely dark environments [77] (such as far below the photic zones in the oceans [18]).

To harvest the small amount of light energy available, these bacteria possess large membranous sacks, called chlorosomes, each containing about 200 000 bacteriochlorophyll (BChl) *c* molecules [78]. In these organisms, harvested excitation energy is transported from the baseplate of a chlorosome to reaction centres through the FMO complexes [76]. The FMO complexes therefore act as molecular wires for excitation energy rather than light-harvesters themselves. The photosynthetic apparatus of green sulphur bacteria is shown in Fig. 6.3.

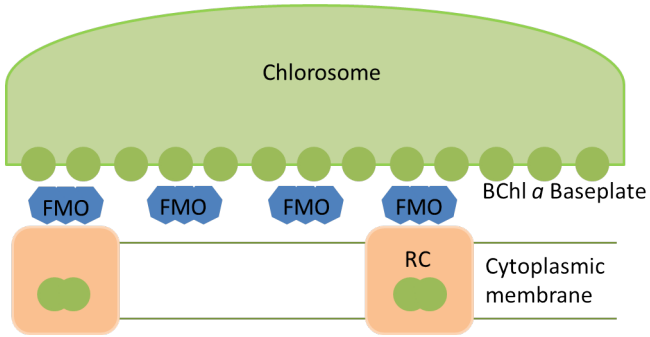

Figure 6.3: The photosynthetic apparatus of green sulphur bacteria.

The FMO-complex is a trimeric complex in which each monomer contains seven BChl *a* molecules arranged as shown in Fig. 6.4 [76].[1]

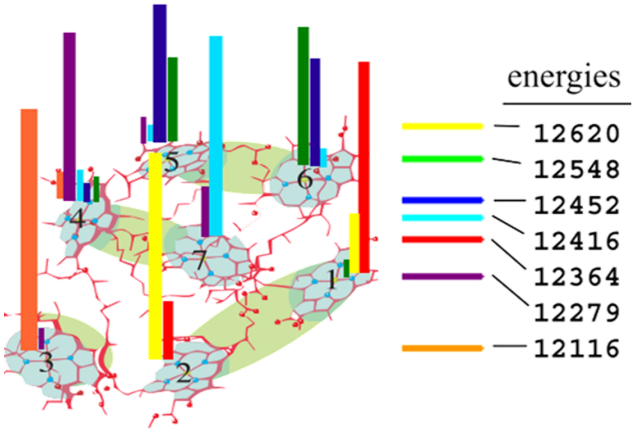

Figure 6.4: The seven chlorophyll *a* molecules in an FMO monomer and their contributions to the exciton states (of which the energies are shown on the right). Taken from Ref. [68] ©(2008)National Academy of Sciences, U.S.A..

[1]There is strong evidence for the presence of an eighth chlorophyll molecule in FMO [79], but the importance of this chlorophyll is still unclear [80, 81]. As is done in most research papers, we will consider the FMO monomer as consisting of seven chlorophyll molecules.

UNIVERSITEIT VAN PRETORIA
UNIVERSITY OF PRETORIA
YUNIBESITHI YA PRETORIA

6.2.1 Single-exciton dynamics

It is thought that the orientation of FMO is such that BChls 1 and 6 are nearest to the baseplate and BChls 3 and 4 are linked to the reaction centre [82]. It is natural to expect, therefore, that the excitation from the chlorosome will excite an initial state in FMO for which excitation is predominantly delocalised over sites 1 and 6. Since the exact initial state is not known, we simulated the dynamics of systems in which only site 1, or only site 6, is initially excited. Site energies and couplings (calculated for the trimeric structure of FMO in the green sulphur bacterium *Chlorobium tepidum*) were obtained from Ref. [83]. The site-basis Hamiltonian is shown in Appendix C. We used a reorganisation energy of 35 cm^{-1}. This reorganisation energy, which is also used by Ishizaki and Fleming [82], was found as best-fit parameter by Read et al. for the green sulphur bacterium *Prosthecochloris aestuarii* [84]. The positions of pigment molecules are almost identical in *P. aestuarii* and *C. tepidum* [85], but the significant spectral differences [85] might be an indication of different average reorganization energies. Like Ishizaki and Fleming [82], we will assume the difference in reorganisation energies between these two bacterial species to be negligible. According to Ishizaki and Fleming [82], a wide range of bath correlation times (ranging from 35 to 166 fs) is reported in literature. Since the Markov approximation is invalid for long correlation times [82], we chose $\tau_c = 35$ fs.

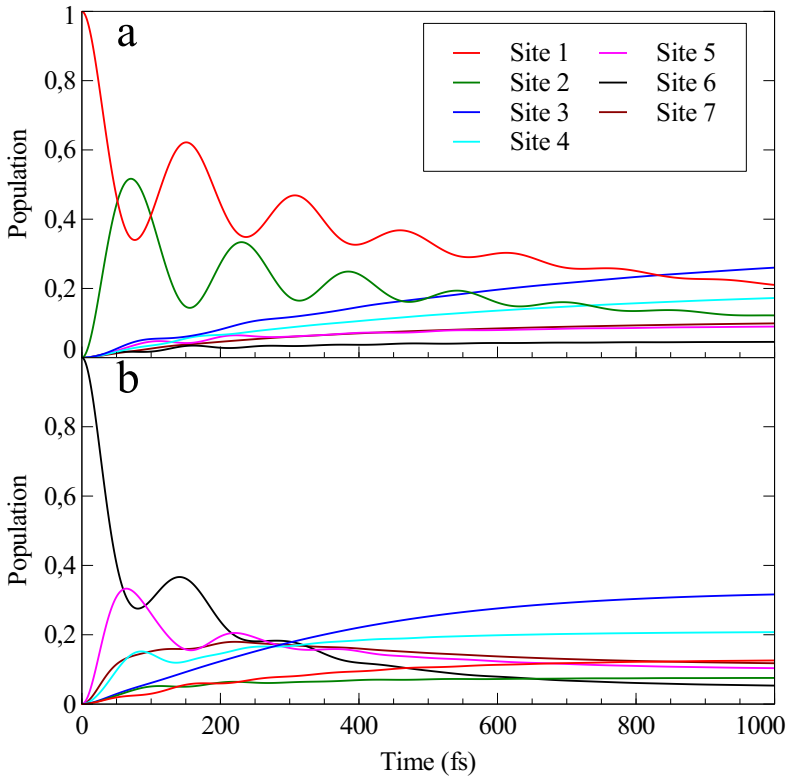

Figure 6.5: Site dynamics of the FMO complex at 300 K for the initial states **a**) $|1\rangle$ and **b**) $|6\rangle$.

The dynamics in Fig. 6.5 agree qualitatively well with the dynamics obtained by Ishizaki and Fleming [82] using a hierarchical equations approach (Section 2.7.4). The dynamics obtained with our secular Redfield method shows slightly faster relaxation to equilibrium than what was obtained by Ishizaki and Fleming. This is a known artefact of the secular Redfield model [62,63]. For the initial state in which only site 1 is excited, our model also predicts coherent oscillations in the populations of sites 1 and 2 over a much longer time-scale than what was found in Ref. [82]. While the latter model predicts coherent oscillations in the populations of sites 1 and 2 lasting about 300 fs, our model predicts these oscillations to last for about 700 fs. This difference is likely due to the failure of the perturbative

UNIVERSITEIT VAN PRETORIA
UNIVERSITY OF PRETORIA
YUNIBESITHI YA PRETORIA

bath-coupling assumption: In Redfield theory, coupling of the system to the bath is treated as a perturbation (see Chapter 3) and $\lambda << V_{mn}$ should therefore hold. The reorganisation energy of 35 cm^{-1} that was used to calculate the dynamics in Fig. 6.5, however, is of the same order as the coupling between sites (see appendix C). The secular Redfield theory apparently over-estimates the coherence between sites when $\lambda \approx V_{mn}$.

From Fig. 6.5**a** it is clear that excitation is transferred from the initial state along the pathway: $1 \rightarrow 2 \rightarrow 3$, corresponding to what was found experimentally by two-dimensional spectroscopy [86]. If site 6 was excited initially, energy transfer proceeds along the path $6 \rightarrow 5{,}7 \rightarrow 4 \rightarrow 3$, which also corresponds to the results of 2D-spectroscopy [86].

The site energy of BChl 2 is higher than the site energy of BChl 1. Excitation trapping on site 1 is avoided, however, by delocalisation of excitation between sites 1 and 2 [82]. In order for energy to be transferred back to site 1 from site 3 (i.e., in the opposite direction as is biologically favourable), the large energy barrier between sites 3 and 2 would have to be overcome [82]. In this pathway, BChl 2 acts as an energy *rectifier*, prohibiting energy backflow from the reaction centre. The energy of BChl 6 is higher than that of the baseplate BChls [82] and backflow of excitation to the baseplate is therefore energetically favoured. Such backflow to the baseplate is reduced by the fast delocalisation of excitation over BChls 6, 5 and 7 [82].

We noted earlier that the secular Redfield model grossly overestimates the time-scale over which coherent oscillations in the populations of sites 1 and 2 are present. Modified Redfield theory, however, still predicts oscillations in some sites to last up to 400 fs at physiological temperatures [82]. Some researchers think that coherent energy transfer (i.e., oscillations in populations) might have important implications for photosynthetic energy transfer [87, 88]. The long-lasting coher-

UNIVERSITEIT VAN PRETORIA
UNIVERSITY OF PRETORIA
YUNIBESITHI YA PRETORIA

ence between sites (of which coherence between sites 1 and 2 is most obvious) is consequently often discussed in literature. In Fig. 6.5, however, coherence between sites 1 and 2 does not seem to play any role: It is clear from Fig. 6.5 that energy transfer to the reaction centre is much slower for the pathway $1 \rightarrow 2 \rightarrow 3$ than for the pathway $6 \rightarrow 5{,}7 \rightarrow 4 \rightarrow 3$ (in which sites 1 and 2 do not play a significant role). The same is true for dynamics predicted by the modified Redfield model [82]. This raises the question of what biological importance sites 1 and 2 have. We simulated the dynamics of FMO with sites 1 and 2 omitted (and all parameters the same as what was used to obtain Fig. 6.5). For this simulation, the dynamics of all sites (except the omitted sites, of course) were quantitatively very similar to the dynamics in Fig. 6.5**b**. From this, it seems as though sites 1 and 2 are redundant...

One possible explanation for the presence of sites 1 and 2 is the following. Site 1 has a lower energy than the baseplate BChls whereas the energy of site 6 is higher than that of the baseplate BChls. Perhaps the existence of two excitation transfer pathways (one of which attracts much excitation, but is slow, and one of which is fast but has a high initial energy barrier) provides the optimal balance.

It might also be possible that erroneous results (due to the limitations of Redfield theory) conceal the functions of pigments 1 and 2. After all, as we noted earlier, coupling to the bath is not weak in FMO and the Redfield dynamics are consequently not necessarily accurate. The same questions about the biological importance of these pigments, however, can be raised from results obtained with modified Redfield theory [82], for which greater coupling to the bath is allowed. It is also possible that the site energies, couplings, reorganisation energy or correlation time (which, as we mentioned above, is reported with a wide range in literature) might be wrong.

The FMO complex is a small part of a large light-harvesting machinery, and we

UNIVERSITEIT VAN PRETORIA
UNIVERSITY OF PRETORIA
YUNIBESITHI YA PRETORIA

cannot expect to find all functions of FMO by only considering the dynamics of the isolated complex. Perhaps pigments 1 and 2 are not directly important for light harvesting; maybe they are necessary for providing the FMO complex with a specific structure, for example. While determining the importance of pigments 1 and 2 in FMO is by no means the purpose of this text, yet another possibility (which is implicated by the excitation dynamics in isolated FMO) is discussed in the next section.

6.2.2 Two-exciton dynamics

As an example of two-exciton dynamics, we consider the double-excitation of FMO (Fig. 6.6). The same parameters were used as for Fig. 6.5. The dynamics of an individual site were obtained by summing over two-excitation states containing that site. We chose the initial state such that both sites 1 and 6 are fully occupied (notice that the total site population is now equal to two).

In Fig. 6.6, it is clear that coherent oscillations are present in the populations of all sites up to 400 fs. This is an indication that all sites participate in a wavelike transfer of energy. It is also clear that the oscillations in the populations of sites 1 and 2 correlate with the populations of other sites. This suggests that excitons are delocalised over larger clusters than in the single-exciton case (where the excitons on sites 1 and 2 were completely decoupled from other excitons). This fact is confirmed in Ref. [68].

Habitats of green sulphur bacteria are diverse. As described above, some of these bacteria exist far below the ocean surface, but many species are abundant at a depth of six metres in lakes [89], where light intensity is presumably much higher than the intensity from black smokers. Green sulphur bacteria belong to a physiologically uniform group [90]. The absorption spectrum of a green sul-

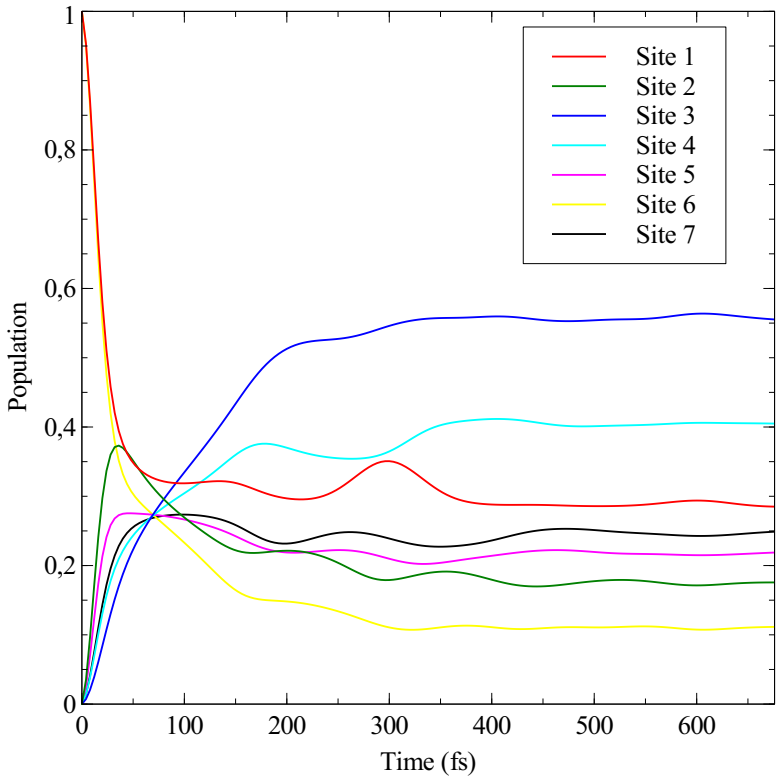

Figure 6.6: The two-exciton dynamics in FMO with an initial state $|(1,6)\rangle$ at 77 K. The populations of individual sites are shown.

phur bacterium is always one of two types: that represented by *C. tepidum* or that represented by *P. aestuarii* [91]. Since the positions of pigment molecules in the FMO complex of these two bacteria are almost identical (see Section 6.2.1), it is reasonable to expect the FMO complexes of all green sulphur bacteria to be very similar. This may lead one to the hypothesis that the presence of BChls 1 and 2 is important only in those green sulphur bacteria that live in much more luminous conditions, where double-excitation may be possible.

If we assume that chlorosomes of green sulphur bacteria, living six metres below the surface of a lake, absorb all incident radiation and that light is attenuated by about 50% after travelling to a depth of six metres (as is the case in mid-latitude

ocean water [92]), it can be calculated that about 5×10^5 photons are absorbed by the chlorosomes per second. There are a couple of tens of FMO complexes per chlorosome [93]. Assuming 50 FMO complexes per chlorosome, each FMO complex receives about 1×10^4 excitations per second. If the reaction centres had infinitesimally short cycles, the single-exciton relaxation time of $\sim$ 1ps would therefore be so fast that single excitations would be transferred to the reaction centres much faster than new excitations are absorbed by FMO from the chlorosomes, and the faster two-exciton relaxation rate would not add significantly to the transfer efficiency. In reality, the reaction centre cycles (the time it takes before the next excitation can be absorbed) is about 10 ms for PS I [94] (which is similar to the reaction centres of green sulphur bacteria [95]).

After an excitation is accepted by a reaction centre, the reaction centre is therefore closed for about 10 ms. From the discussion above, it follows that about 100 excitations are absorbed per FMO complex during this time. These extra excitations wander through the light-harvesting complex until their energy is dissipated by another loss channel such as fluorescence or annihilation. Not much is known about the lifetime of BChls in intact cells, but BChls in isolated chlorosomes are thought to have fluorescence lifetimes shorter than 30 ps [96]. If we assume that this lifetime is also valid for BChls in living green sulphur bacteria, the fluorescence decay rate is much faster than the rate at which new excitations are absorbed.

Even if the lifetimes of excitations are significantly longer in living bacteria than in isolated chlorosomes, excitations would be annihilated very efficiently through the process of singlet-triplet annihilation: With a probability of about 10% [97], any (singlet) excitation can undergo intersystem crossing (invert the spin of one of the BChl electrons) to form a triplet state before the excitation loses its energy through fluorescence. This triplet state has a lifetime of about 1 ms [98] and

UNIVERSITEIT VAN PRETORIA
UNIVERSITY OF PRETORIA
YUNIBESITHI YA PRETORIA

quenches singlet excitations efficiently through the reaction (see Refs. [57, 69] for discussions of annihilation)

$$S_1 + T_1 \rightarrow S_0 + T_n,$$

where S_1 and S_0 are the first excited singlet and ground electronic states of BChl, respectively, and T_1 and T_n are the first and n^{th} excited triplet level, respectively. T_n is rapidly converted back to T_1 [99], which can then annihilate another singlet excitation. Absorbed excitations therefore have a high probability of being rapidly annihilated by triplet states.

Given the short lifetimes of excitations and the efficient annihilation by triplet states, it is unlikely that more than one (singlet) excitation will be present in an FMO complex when a reaction centre opens. Even if multiple excitations were present, the small increase in relaxation rate would still be insignificant compared to the long reaction centre cycle. Apparently, the active roles of pigments 1 and 2 in two-exciton relaxation does not explain their biological significance.

6.3 LHCII

LHCII forms part of the PSII superstructure (see Section 1.4.1) and is the main light harvester for the initial steps of the electron transport chain in plants (Section 1.2.1). LHCII is a trimer in which each monomer consists of fourteen chlorophyll molecules (eight chlorophyll *a*'s and six chlorophyll *b*'s), four carotenoids and a protein backbone [48]. The carotenoid molecules are involved in light harvesting, but their main function is photoregulation [49]. We therefore considered only the exciton dynamics of the chlorophyll molecules (as if the carotenoid molecules were not present).

The site energies of chlorophylls (Chls) in LHCII were obtained from Ref. [100] and the couplings were obtained from Refs. [101] and [102]. The Hamiltonian is shown in Appendix C. These couplings and site energies are that of an LHCII monomer (i.e., it is assumed that coupling between pigments in different monomers is zero). We used a reorganisation energy of 220 cm^{-1} and correlation time of 15 fs, as employed by Kreisbeck and Aspuru-Guzik [103]. We assumed an initial state with equal (classical) contribution of all exciton states. Since one would expect excitons in a narrow energy range (like in LHCII) to be represented equally in an ensemble after excitation by broad light, this assumption is not unphysical. The dynamics from this initial state is shown in Fig. 6.7. The participation of pigment wavefunctions to exciton states are shown in Table 6.1.

The dynamics in Fig. 6.7 shows the same general trend as was found by Novoderezhkin et al. [100] (they used a Modified Redfield approach). Populations of excitons with predominant Chl *a* character (see Table 6.1) are increasing functions whereas populations of excitons with predominant Chl *b* character generally decrease. These trends are manifestations of the fact that excitons in LHCII are delocalised over small clusters of 2-3 pigment molecules, each cluster consisting either mainly of Chl *a* or of Chl *b* (Table 6.1). Since the site energies of the Chls *b* are higher than the site energies of the Chls *a*, the excitons with strong Chl *b* character lose excitation to the Chl *a* excitons. Only excitons 6 and 7 have strong contribution from both Chl *a* (Chl 3) and Chl *b* (Chl 14) molecules, and the populations of these excitons remain essentially static.

The evolution of populations of excitons 5 and 8 differ significantly from monotonic behaviour. Exciton 5 consists mainly of Chls 11 and 12. The population of this exciton shows the fastest initial decay and the population of exciton 1 (which is delocalised over Chls 10, 11 and 12) shows the fastest initial increase. This behaviour is probably an indication of the fast equilibration of population within the

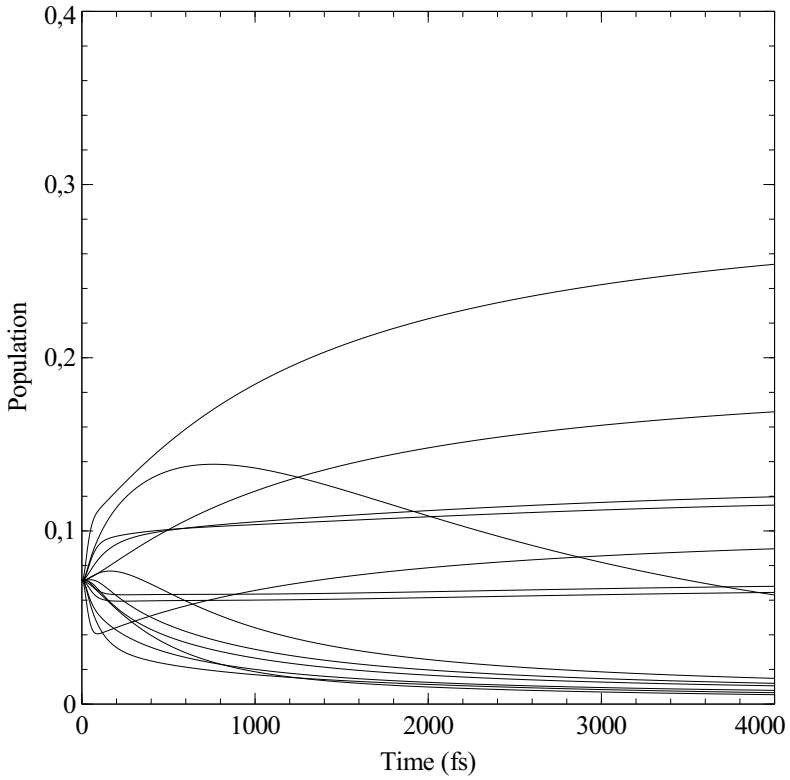

Figure 6.7: The exciton dynamics in a monomer of LHCII. Exciton states are numbered in the order their populations appear at 4000 fs, with exciton 1 having the lowest energy (i.e., highest population).

strongly coupled cluster Chl 10-11-12 (the cluster over which the lowest-energy exciton is delocalised). Exciton 8 is localised, almost completely, on Chl 4 (a Chl *a*), which is strongly coupled to Chls *b* 6 and 7. Chl 4 is only weakly coupled to all other Chls in LHCII (see Table 6.1). Because of its lower energy, exciton 8 is therefore rapidly supplied with excitation by excitons with strong Chl 6 or Chl 7 character (from Table 6.1, excitons 10-13). Its weak coupling to other Chls accounts for the long decay time of exciton 8. Novoderezhkin et al. [100] mentions that exciton 8 is a good candidate for the bottleneck state suggested in experimental studies [104–106]. Our result agrees well with this observation!

Table 6.1: Participation of site-basis wave functions to exciton states of LHCII. The type of Chl (*a* or *b*) is indicated next to the pigment numbers. Total participation is normalised to 1000 and only values greater or equal to 1 were retained.

Pigments	**Excitons**													
	1	2	3	4	5	6	7	8	9	10	11	12	13	14
1 *b*	-	-	2	-	1	-	-	-	-	-	-	1	11	985
2 *a*	2	1	931	25	12	17	8	-	-	-	1	1	-	2
3 *a*	-	2	21	1	-	569	383	-	-	3	16	5	-	-
4 *a*	-	-	-	-	-	-	-	964	-	3	-	-	31	1
5 *b*	-	-	-	-	-	-	-	-	973	19	5	1	2	-
6 *b*	-	-	-	-	-	-	-	29	5	17	-	5	935	10
7 *b*	-	-	-	-	-	-	-	6	20	887	66	4	16	1
8 *b*	1	3	-	-	-	-	-	-	2	5	224	760	4	1
9 *b*	-	-	4	-	-	14	8	-	-	67	687	220	-	-
10 *a*	121	862	1	4	7	-	1	-	-	-	1	3	-	-
11 *a*	415	33	9	2	540	-	-	-	-	-	-	-	-	1
12 *a*	462	95	2	4	437	-	-	-	-	-	-	-	-	-
13 *a*	-	4	27	856	2	47	65	-	-	-	-	-	-	-
14 *a*	-	-	2	109	2	353	534	-	-	-	-	-	-	-

UNIVERSITEIT VAN PRETORIA
UNIVERSITY OF PRETORIA
YUNIBESITHI YA PRETORIA

Conclusion

Without photosynthesis, the vast majority of life today could not exist! During the process of photosynthesis, energy from sunlight is absorbed by pigment molecules in light-harvesting complexes, very efficiently transported to a molecular reaction centre and ultimately converted to chemical energy.

The light-harvesting complexes consist of pigment molecules that are kept in place by an intricate protein environment. In these complexes, pigment molecules are close to one another and interact significantly through their transition dipole moments. This strong interaction leads to the delocalisation of excitation over clusters of pigment molecules. These states of delocalised excitation are called excitons. The formation of exciton states are advantageous for light-harvesting: they allow different diffusion paths to be explored simultaneously and energy traps to be avoided.

Excitons couple to the large number of vibrational states of the pigment-protein conglomerate. As it is often done in literature, we assume that the vibrations can be modelled as a bath of infinitely many harmonic oscillators, each coupled linearly to an exciton state. The bath causes relaxation of the electronic degrees of freedom to an equilibrium (Boltzmann) state.

When the coupling between excitons and the bath is much weaker than the coupling between pigment molecules, the Redfield equation gives an accurate descrip-

UNIVERSITEIT VAN PRETORIA
UNIVERSITY OF PRETORIA
YUNIBESITHI YA PRETORIA

tion of exciton dynamics.

It is possible for a system to contain more than one excitation. The quantum states of such a system are called two-exciton states. In the weak bath-coupling limit, the dynamics of two-exciton states are also desribed by the Redfield equation. In a system for which bath coupling is not weak (i.e., for a system in the Förster regime), it is possible to express two-excitation dynamics as the evolution of the populations of individual sites—exactly at high temperatures and approximately at finite temperatures. It seems unlikely that a similar description is possible for a system with two delocalised excitations (excitons).

We calculated the exciton dynamics of three systems: a six-pigment ring, a monomer of the Fenna-Matthews-Olson complex of green sulphur bacteria and a monomer of LHCII, the main light-harvester in green plants. These dynamics were calculated using the secular Redfield equation.

For the six-pigment ring, relaxation of population, decay of coherence between exciton states and coherent population oscillations could be observed.

For FMO, our results compared well with the results of a different simulation from literature. The secular Redfield model also predicts excitation transfer pathways that were proposed in experimental studies. The secular Redfield theory appears to overestimate the rate of relaxation and the lifetime of coherent oscillations in populations of exciton states. We observe that the biological role of pigment molecules 1 and 2 in FMO is unclear.

For LHCII, our results compare well with the results from other simulations in literature. A bottleneck state, which was implicated in experimental studies and observed in other simulations, can also be identified from the dynamics which we calculated.

UNIVERSITEIT VAN PRETORIA
UNIVERSITY OF PRETORIA
YUNIBESITHI YA PRETORIA

Appendices

UNIVERSITEIT VAN PRETORIA
UNIVERSITY OF PRETORIA
YUNIBESITHI YA PRETORIA

Appendix A

List of Abbreviations

ATP	Adenosine triphosphate
NADPH	Nicotinamide adenine dinucleotide phosphate
PS I/II	Photosystem I / Photosystem II
CP	Chlorophyl protein
LHCII	Main light-harvesting complex II of plants
FRET	Förster energy resonance transfer
FMO	Fenna-Matthews-Olson complex
Chl	Chlorophyll
BChl	Bacteriochlorophyll
LH 1/2	Light-harvesting complexes of purple bacteria

UNIVERSITEIT VAN PRETORIA
UNIVERSITY OF PRETORIA
YUNIBESITHI YA PRETORIA

Appendix B

Towards a single-exciton description of two-exciton dynamics

Let the population of the two-exciton state, with one exciton on site α and the other on site β, be $P_{\alpha\beta} = P_{\beta\alpha}$. Let P_α be the population of site α.

$$\begin{aligned} P_\alpha &= \sum_{\gamma\neq\alpha} P_{\alpha\gamma} \\ 2\frac{d}{dt}P_\alpha &= 2\sum_{\gamma\neq\alpha}\frac{d}{dt}P_{\alpha\gamma} \\ &= \sum_{\gamma\neq\alpha}\Big[-P_{\alpha\gamma}\big(\sum_l\sum_m R_{lm\leftarrow\alpha\gamma}\big) + \big(\sum_l\sum_m P_{lm}R_{\alpha\gamma\leftarrow lm}\big)\Big], \end{aligned} \tag{B.1}$$

where

$$\begin{aligned} R_{AB\leftarrow CD} &= (1-\delta_{AB})(1-\delta_{CD})\times \\ &\quad (\delta_{AC}R_{BD} + \delta_{AD}R_{BC} + \delta_{BC}R_{AD} + \delta_{BD}R_{AC}). \end{aligned} \tag{B.2}$$

In equation B.2, R_{AB} is the single-exciton transfer rate from site B to site A. The terms $(1-\delta_{AB})$, $(1-\delta_{CD})$ ensure that rates such as $R_{11\leftarrow 12}$ are zero. The last term in equation B.1 is responsible for a couple of things:

1. It converts the two-exciton rates to single-exciton rates. Suppose $A = C$, say $A = C = 1$, $B = 2$, $D = 3$. Then

$$\begin{aligned} R_{AB\leftarrow CD} &= R_{12\leftarrow 13} \\ &= \delta_{AC}R_{BD} + \delta_{AD}R_{BC} + \ldots \\ &= \delta_{11}R_{23} \\ &= R_{23}. \end{aligned}$$

2. It prohibits transfers from a state to itself.

$$\begin{aligned} R_{12\leftarrow 12} &= R_{12\leftarrow 21} \\ &= R_{22} + R_{11} \\ &= 0 \end{aligned}$$

3. It allows only transfers where only one excitation changes site per transfer.

$$R_{12\leftarrow 45} = 0.$$

Now, back to equation B.1:

$$
\begin{aligned}
2\frac{d}{dt}P_\alpha = \sum_{\gamma\neq\alpha}\sum_{l}\sum_{m}\big[& -P_{\alpha\gamma}(1-\delta_{lm})(1-\delta_{\alpha\gamma})(\delta_{l\alpha}R_{m\gamma}+\delta_{l\gamma}R_{m\alpha}+\delta_{m\alpha}R_{l\gamma}+\delta_{m\gamma}R_{l\alpha}) \\
& +P_{lm}(1-\delta_{lm})(1-\delta_{\alpha\gamma})(\delta_{l\alpha}R_{\gamma m}+\delta_{l\gamma}R_{\alpha m}+\delta_{m\alpha}R_{\gamma l}+\delta_{m\gamma}R_{\alpha l})\big] \\
= \sum_{\gamma\neq\alpha}\Bigg[& -\sum_{l}\big[P_{\alpha\gamma}(1-\delta_{l\alpha})(1-\delta_{\alpha\gamma})R_{l\gamma}+P_{\alpha\gamma}(1-\delta_{l\gamma})(1-\delta_{\alpha\gamma})R_{l\alpha}\big] \\
& -\sum_{m}\big[P_{\alpha\gamma}(1-\delta_{\alpha m})(1-\delta_{\alpha\gamma})R_{m\gamma}+P_{\alpha\gamma}(1-\delta_{\gamma m})(1-\delta_{\alpha\gamma})R_{m\alpha}\big] \\
& +\sum_{l}\big[P_{l\alpha}(1-\delta_{l\alpha})(1-\delta_{\alpha\gamma})R_{\gamma l}+P_{l\gamma}(1-\delta_{l\gamma})(1-\delta_{\alpha\gamma})R_{\alpha l}\big] \\
& +\sum_{m}\big[P_{\alpha m}(1-\delta_{\alpha m})(1-\delta_{\alpha\gamma})R_{\gamma m}+P_{\gamma m}(1-\delta_{\gamma m})(1-\delta_{\alpha\gamma})R_{\alpha m}\big]\Bigg].
\end{aligned}
$$

The sum, S_1, of all the terms in the first column above is

$$
\begin{aligned}
S_1 &= -\sum_{l\neq\alpha}\sum_{\gamma\neq\alpha}P_{\alpha\gamma}R_{l\gamma}-\sum_{m\neq\alpha}\sum_{\gamma\neq\alpha}P_{\alpha\gamma}R_{m\gamma}+\sum_{l\neq\alpha}\sum_{\gamma\neq\alpha}P_{l\alpha}R_{\gamma l}+\sum_{m\neq\alpha}\sum_{\gamma\neq\alpha}P_{\alpha m}R_{\gamma m} \\
&= \sum_{l\neq\alpha}\sum_{\gamma\neq\alpha}(-P_{\alpha\gamma}R_{l\gamma}-P_{\alpha\gamma}R_{l\gamma}+P_{l\alpha}R_{\gamma l}+P_{\alpha l}R_{\gamma l}) \\
&= \sum_{l\neq\alpha}\sum_{\gamma\neq\alpha}(-2P_{\alpha\gamma}R_{l\gamma}+2P_{\alpha l}R_{\gamma l}) \\
&= \sum_{l\neq\alpha}\sum_{\gamma\neq\alpha}(-2P_{\alpha\gamma}R_{l\gamma}+2P_{\alpha\gamma}R_{l\gamma}) \\
&= 0.
\end{aligned}
$$

The sum, S_2, of all terms in the second column is:

$$\begin{aligned} S_2 &= \sum_{\gamma\neq\alpha}\sum_{l\neq\gamma}\left[-P_{\alpha\gamma}R_{l\alpha} - P_{\alpha\gamma}R_{l\alpha} + P_{l\gamma}R_{\alpha l} + P_{\gamma l}R_{\alpha l}\right] \\ &= \sum_{\gamma\neq\alpha}\sum_{l\neq\gamma}\left[-2P_{\alpha\gamma}R_{l\alpha} + 2P_{l\gamma}R_{\alpha l}\right] \\ &= \sum_{l}\left[-2R_{l\alpha}\sum_{\gamma\neq\alpha,l}P_{\alpha\gamma} + 2R_{\alpha l}\sum_{\gamma\neq\alpha,l}P_{l\gamma}\right] \\ &= 2\sum_{l}\left[-R_{l\alpha}(P_\alpha - P_{\alpha l}) + R_{\alpha l}(P_l - P_{l\alpha})\right]. \end{aligned}$$

Therefore:

$$2\frac{d}{dt}P_\alpha = 2\sum_{l}\left[-R_{l\alpha}(P_\alpha - P_{\alpha l}) + R_{\alpha l}(P_l - P_{l\alpha})\right].$$

If the approximation $P_{\alpha l} = P_{l\alpha} = P_l P_\alpha$ is made, then

$$\frac{d}{dt}P_\alpha = \sum_{l\neq\alpha}P_l(1-P_\alpha)R_{\alpha l} - P_\alpha\sum_{l\neq\alpha}(1-P_l)R_{\alpha l}.$$

Appendix C

FMO and LHCII Hamiltonians

In the Hamiltonians below, the site energies (in cm^{-1}) are given on the diagonals and coupling between sites on the off-diagonals.

FMO

$$H = \begin{bmatrix} 12410 & -87.7 & 5.5 & -5.9 & 6.7 & -13.7 & -9.9 \\ -87.7 & 12530 & 30.8 & 8.2 & 0.7 & 11.8 & 4.3 \\ 5.5 & 30.8 & 12210 & -53.5 & -2.2 & -9.6 & 6.0 \\ -5.9 & 8.2 & -53.5 & 12320 & -70.7 & -17 & -63.3 \\ 6.7 & 0.7 & -2.2 & -70.7 & 12480 & 81.1 & -1.3 \\ -13.7 & 11.8 & -9.6 & -17 & 81.1 & 12630 & 39.7 \\ -9.9 & 4.3 & 6.0 & -63.3 & -1.3 & 39.7 & 12440 \end{bmatrix}$$

LHCII

$$H = \begin{bmatrix} 15890 & 36 & -5 & -3 & 1 & -2 & -3 & 3 & 4 & -5 & 20 & 2 & -8 & 2 \\ 36 & 15160 & 15.0 & 6.0 & 0.0 & 5.0 & 6 & -6 & -24 & -5 & 1 & 8 & -2 & 0 \\ -5 & 15 & 15283 & -1.0 & 0.0 & -4.0 & 6 & 4 & 72 & 7 & -1 & 1 & 1 & -5 \\ -3 & 6 & -1 & 15460 & 4.0 & 71.0 & 24 & -4 & -2 & 0 & -3 & 3 & 2 & -3 \\ 1 & 0 & 0 & 4 & 15679 & 9 & -4 & -4 & 0 & 1 & 1 & -2 & -1 & 0 \\ -2 & 5 & -4 & 71 & 9 & 15851 & 16 & -5 & 2 & 0 & -2 & 2 & 2 & -2 \\ -3 & 6 & 6 & 24 & -4 & 16 & 15712 & -4 & -5 & 1 & -2 & 3 & 3 & -3 \\ 3 & -6 & 4 & -4 & -4 & -5 & -4 & 15763 & 24 & 43 & 5 & -1 & -2 & 1 \\ 4 & -24 & 72 & -2 & 0 & 2 & -5 & 24 & 15721 & -2 & 4 & -1 & -2 & 2 \\ 5 & -5 & 7 & 0 & 1 & 0 & 1 & 43 & -2 & 15073 & -2613 & 6 & 6 & -1 \\ 20 & 1 & -1 & -3 & 1 & -2 & -2 & 5 & 4 & -26 & 15115 & 99 & -3 & 1 \\ 2 & 8 & 1 & 3 & -2 & 2 & 3 & -1 & -1 & 13 & 99 & 15097 & 0 & 0 \\ -8 & -2 & 1 & 2 & -1 & 2 & 3 & -2 & -2 & 6 & -3 & 0 & 15175 & -36 \\ 2 & 0 & -5 & -3 & 0 & -2 & -3 & 1 & 2 & -1 & 1 & 0 & -36 & 15264 \end{bmatrix}$$

Bibliography

[1] U. Steger, W. Achterberg, K. Blok *et al.*, *Sustainable Development and Innovation in the Energy Sector*. Springer Science & Business Media, 2005.

[2] International Energy Agency, "2014 Key World Energy Statistics," p. 82. [Online]. Available: http://www.iea.org/publications/freepublications/publication/KeyWorld2014.pdf

[3] N. A. Campbell, J. B. W. Reece, L. A. Urry *et al.*, *Biology*, 8th ed. San Francisco: Pearson, Benjamin Cummings, 2008.

[4] Worldometers, "Current World Population." [Online]. Available: http://www.worldometers.info/world-population/

[5] W. S. Fyfe, H. Puchelt, and M. Taube, *The Natural Environment and the Biogeochemical Cycles*, ser. The Handbook of Environmental Chemistry. Springer Berlin Heidelberg, 2013.

[6] H. Jones, "Design Rules for Space Life Support Systems," in *Int. Conf. Environ. Syst.*, jul 2003, p. 16. [Online]. Available: http://papers.sae.org/2003-01-2356/

[7] C. Leuschner, "Vegetation and Ecosystem," in *Veg. Ecol.*, 2nd ed., E. Van der Maarel and J. Franklin, Eds., ch. 10. West Sussex: John Wiley & Sons, 2013.

[8] P. Hobson, *The Rumen Microbial Ecosystem*, P. N. Hobson and C. S. Stewart, Eds. Dordrecht: Springer Netherlands, 1997.

[9] M. Zarnkow, "Encyclopedia of Food Microbiology," in *Encycl. Food Microbiol.*, 2nd ed., C. A. Batt and M.-L. Tortolello, Eds., ch. Bacteriocins. Elsevier, 2014.

[10] W. Lewis and J. Lowenfels, *Teaming with Microbes: The Organic Gardener's Guide to the Soil Food Web*, revised ed. Timber Press, 2010.

[11] T. H. Nash, *Lichen Biology*, 2nd ed. Cambridge University Press, 2008.

[12] J. P. Zehr and R. M. Kudela, "Photosynthesis in the Open Ocean," *Science*, vol. 326, pp. 945–946, 2009.

[13] J. Schopf, *Ecology of Cyanobacteria II*, B. A. Whitton, Ed. Dordrecht: Springer Netherlands, 2012.

[14] L. Brey, "Acclimation of Kelp photosynthesis to seasonal changes in the underwater radiation regime of an Artic Fjord system," Ph.D. dissertation, University of Bremen, 2009.

[15] S. M. Marshall and A. P. Orr, "The Photosynthesis of Diatom Cultures in the Sea," *J. Mar. Biol. Assoc.*, vol. 15, pp. 321–360, 1928.

[16] P. Tett, *The photic zone*, P. J. Herring, Ed. Cambridge University Press, 1990.

[17] C. L. Van Dover, *The Ecology of Deep-sea Hydrothermal Vents*. Princeton University Press, 2000.

[18] J. T. Beatty, J. Overmann, M. T. Lince *et al.*, "An obligately photosynthetic bacterial anaerobe from a deep-sea hydrothermal vent." *Proc. Natl. Acad. Sci. U. S. A.*, vol. 102, pp. 9306–9310, 2005.

[19] D. Chivian, E. L. Brodie, E. J. Alm *et al.*, "Environmental Genomics Reveals a Single-Species Ecosystem Deep Within Earth," *Science*, vol. 322, pp. 275–278, 2008.

[20] I. Lowe, *Artificial Photosynthesis: From Basic Biology to Industrial Application*, A. F. Collings and C. Critchley, Eds. Weinheim: Wiley, 2005.

[21] R. Razeghifard, *Natural and Artificial Photosynthesis: Solar Power as an Energy Source*. Hoboken: John Wiley & Sons, 2013.

[22] K. Collins, " 'Artificial leaf' could power communities for the future." [Online]. Available: http://www.wired.co.uk/news/archive/2015-08/17/artificial-leaf-photosynthesis-could-replace-fossil-fuels

[23] G. R. Fleming, G. S. Schlau-Cohen, K. Amarnath *et al.*, "Design principles of photosynthetic light-harvesting," *Faraday Discuss.*, vol. 155, pp. 27–41, 2012.

[24] D. Borghino, "Artificial photosynthesis breakthrough turns CO2 emissions into plastics and biofuel." [Online]. Available: http://www.gizmag.com/artificial-photosynthesis-creates-biofuel/37160/

[25] R. P. Cantrell, *Redesigning Rice Photosynthesis to Increase Yield*, J. E. Sheehy, B. Hardy, P. L. Mitchell *et al.*, Eds. Amsterdam: Elsevier Science, 2000.

[26] H. Ledford, "Hacked photosynthesis could boost crop yields: Algal enzyme can speed up rate at which plants make food." [Online]. Available: http://www.nature.com/news/hacked-photosynthesis-could-boost-crop-yields-1.15949

[27] G. M. Cooper and R. E. Hausman, *The Cell: A Molecular Approach*. ASM Press, 2004.

[28] J.-D. Rochaix and S. Ramundo, *Plastid Biology*, ser. Advances in Plant Biology, S. Theg and F. A. Wollman, Eds. New Yorck: Springer New York, 2014.

[29] I. D. Denev and I. N. Minkov, *Handbook of Plant and Crop Physiology*, 2nd ed., ser. Books in Soils, Plants, and the Environment, M. Pessarakli, Ed. CRC Press, 2001.

[30] A. R. Crofts, *The Q-cyle - a personal perspective*, ser. Advances in Photosynthesis and Respiration, Govindjee, B. J. T, G. H *et al.*, Eds. Dordrecht: Springer, 2006.

[31] V. V. Klimov, "Discovery of pheophytin function in the photosynthetic energy conversion as the primary electron acceptor of photosystem II," *Photosynth. Res.*, vol. 76, pp. 247–253, 2003.

[32] G. Renger, "Photosynthetic water oxidation to molecular oxygen: Apparatus and mechanism," *Biochim. Biophys. Acta - Bioenerg.*, vol. 1503, pp. 210–228, 2001.

[33] M. Lundberg and P. E. M. Siegbahn, "Theoretical investigations of structure and mechanism of the oxygen-evolving complex in PSII," *Phys. Chem. Chem. Phys.*, vol. 6, pp. 4772–4780, 2004.

[34] P. Mitchell, "Hydrogen Transfer By a Chemi-Osmotic Type," *Nature*, vol. 191, pp. 144–148, 1961.

[35] H. Wang and G. Oster, "Energy transduction in the F1 motor of ATP synthase." *Nature*, vol. 396, pp. 279–282, 1998.

[36] Kanehisa Laboratories, "COMPOUND: C00118." [Online]. Available: http://www.genome.jp/dbget-bin/www_bget?cpd:c00118

[37] E. Lawrence, Ed., *Henderson's Dictionary of Biology*, 14th ed. Essex: Pearson Education, 2008.

[38] A. W. D. Larkum, S. E. Douglas, and J. A. Raven, Eds., *Photosynthesis in Algae*, ser. Advances in Photosynthesis and Respiration. Dordrecht: Springer Netherlands, 2003, vol. 14.

[39] A. Herrero and F. G. Flores, Eds., *The Cyanobacteria: Molecular Biology, Genomics, and Evolution*. Norfolk: Caister Academic Press, 2008.

[40] M. T. Madigan, J. M. Martinko, P. V. Dunlap *et al.*, Eds., *Brock Biology of Microorganisms*, 12th ed. San Francisco: Benjamin Cummings, 2012.

[41] J. Nield and J. Barber, "Refinement of the structural model for the Photosystem II supercomplex of higher plants," *Biochim. Biophys. Acta - Bioenerg.*, vol. 1757, pp. 353–361, 2006.

[42] A. P. Casazza, M. Szczepaniak, M. G. Müller *et al.*, "Energy transfer processes in the isolated core antenna complexes CP43 and CP47 of photosystem II." *Biochim. Biophys. Acta*, vol. 1797, pp. 1606–1616, 2010.

[43] T. M. Bricker and L. K. Frankel, "The structure and function of CP47 and CP43 in Photosystem II," *Photosynth. Res.*, vol. 72, pp. 131–146, 2002.

[44] X. Pan, Z. Liu, M. Li *et al.*, "Architecture and function of plant light-harvesting complexes II," *Curr. Opin. Struct. Biol.*, vol. 23, pp. 515–525, 2013.

[45] Y. E. Chen, Z. Y. Zhao, H. Y. Zhang *et al.*, "Significance of CP29 reversible phosphorylation in thylakoids of higher plants under environmental stresses," *J. Exp. Bot.*, vol. 64, pp. 1167–1178, 2013.

[46] S. de Bianchi, L. Dall'Osto, G. Tognon *et al.*, "Minor antenna proteins CP24 and CP26 affect the interactions between photosystem II subunits and the electron transport rate in grana membranes of Arabidopsis." *Plant Cell*, vol. 20, pp. 1012–1028, 2008.

[47] M. Pribil, M. Labs, and D. Leister, "Structure and dynamics of thylakoids in land plants," *J. Exp. Bot.*, vol. 65, pp. 1955–1972, 2014.

[48] Z. Liu, H. Yan, K. Wang *et al.*, "Crystal structure of spinach major light-harvesting complex at 2.72 Å resolution," *Nature*, vol. 428, pp. 287–292, 2004.

[49] G. Scholes, G. Fleming, a. Olaya-Castro *et al.*, "Lessons from nature about solar light harvesting," *Nat. Publ. Gr.*, vol. 3, pp. 763–774, 2011.

[50] R. Van Grondelle and V. I. Novoderezhkinb, "Quantum effects in photosynthesis," *Procedia Chem.*, vol. 3, pp. 198–210, 2011.

[51] T. C. Yen and Y. C. Cheng, "Electronic coherence effects in photosynthetic light harvesting," *Procedia Chem.*, vol. 3, pp. 211–221, 2011.

[52] G. S. Beddard and G. Porter, "Concentration quenching in chlorophyll," *Nature*, vol. 260, pp. 366–367, 1976.

UNIVERSITEIT VAN PRETORIA
UNIVERSITY OF PRETORIA
YUNIBESITHI YA PRETORIA

[53] A. Chenu and G. D. Scholes, "Coherence in Energy Transfer and Photosynthesis," *Annu. Rev. Phys. Chem.*, vol. 66, pp. 69–96, 2014.

[54] T. Krüger and R. van Grondelle, "Design principles of natural light-harvesting as revealed by single molecule spectroscopy," *Phys. B Condens. Matter*, vol. 480, pp. 7–13, 2016.

[55] H.-P. Breuer and F. Petruccione, *The Theory of Open Quantum Systems*. Oxford University Press, 2002.

[56] L. Valkunas, D. Abramavicius, and T. Mancal, *Molecular Excitation Dynamics and Relaxation: Quantum Theory and Spectroscopy*. John Wiley & Sons, 2013.

[57] H. van Amerongen, L. Valkunas, and R. van Grondelle, *Photosynthetic Excitons*. World Scientific, 2000.

[58] T. Renger, " Absorption of Light, Excitation Energy Transfer and Electron Transfer Reactions," in *Prim. Process. Photosynth. Part 1*, G. Renger, Ed., ch. 2. Cambridge: Royal Society of Chemistry, 2007.

[59] S. Mukamel, *Principles of nonlinear optical spectroscopy*. Oxford University Press, 1995.

[60] M. Yang and G. R. Fleming, "Influence of phonons on exciton transfer dynamics: comparison of the Redfield, Förster, and modified Redfield equations," *Chem. Phys.*, vol. 275, pp. 355–372, 2002.

[61] W. M. Zhang, T. Meier, V. Chernyak *et al.*, "Exciton-migration and three-pulse femtosecond optical spectroscopies of photosynthetic antenna complexes," *J. Chem. Phys.*, vol. 108, pp. 7763–7774, 1998.

[62] A. Ishizaki and G. R. Fleming, "Unified treatment of quantum coherent and incoherent hopping dynamics in electronic energy transfer: Reduced hierarchy equation approach," *J. Chem. Phys.*, vol. 130, 2009.

[63] C. Kreisbeck, T. Kramer, M. Rodriguez *et al.*, "High-Performance Solution of Hierarchical Equations of Motion for Studying Energy Transfer in Light-Harvesting Complexes," *J. Chem. Theory Comput.*, vol. 7, pp. 2166–2174, 2011.

[64] J. Wu, F. Liu, Y. Shen *et al.*, "Efficient energy transfer in light-harvesting systems: optimal temperature, reorganization energy and spatial-temporal correlations," *New J. Phys.*, vol. 12, 2010.

[65] V. May and O. Kühn, *Charge and Energy Transfer Dynamics in Molecular Systems*, 3rd ed. John Wiley & Sons, 2011.

[66] G. Milovanovic, "Density Matrix Formulation," Ph.D. dissertation, Technical University München, 2011. [Online]. Available: http://www.iue.tuwien.ac.at/phd/milovanovic/

[67] J. Olšina and T. Mančal, "Electronic coherence dephasing in excitonic molecular complexes: Role of Markov and secular approximations," *J. Mol. Model.*, vol. 16, pp. 1765–1778, 2010.

[68] D. Abramavicius, D. V. Voronine, and S. Mukamel, "Double-quantum resonances and exciton-scattering in coherent 2D spectroscopy of photosynthetic complexes." *Proc. Natl. Acad. Sci. U. S. A.*, vol. 105, pp. 8525–8530, 2008.

[69] L. Valkunas, E. Akesson, T. Pullerits *et al.*, "Energy migration in the light-harvesting antenna of the photosynthetic bacterium Rhodospirillum rub-

rum studied by time-resolved excitation annihilation at 77 K," *Biophys. J.*, vol. 70, pp. 2373–2379, 1996.

[70] B. Brüggemann and V. May, "Ultrafast laser pulse control of exciton dynamics: A computational study on the FMO complex," *J. Phys. Chem. B*, vol. 108, pp. 10 529–10 539, 2004.

[71] W. M. Zhang, T. Meier, V. Chernyak *et al.*, "Exciton-migration and three-pulse femtosecond optical spectroscopies of photosynthetic antenna complexes," *J. Chem. Phys.*, vol. 108, pp. 7763–7774, 1998.

[72] V. Abramavicius and D. Abramavicius, "Excitation transfer pathways in excitonic aggregates revealed by the stochastic Schrödinger equation," *The Journal of Chemical Physics*, vol. 140, pp. 65 103–65 118, 2014.

[73] J. W. Eaton, "GNU Octave." [Online]. Available: https://www.gnu.org/software/octave/

[74] G. S. Schlau-Cohen, T. R. Calhoun, N. S. Ginsberg *et al.*, "Spectroscopic elucidation of uncoupled transition energies in the major photosynthetic light-harvesting complex, LHCII," *Proc. Natl. Acad. Sci.*, vol. 107, pp. 13 276–13 281, 2010.

[75] F. Müh, D. Lindorfer, M. Schmidt am Busch *et al.*, "Towards a structure-based exciton Hamiltonian for the CP29 antenna of photosystem II," *Phys. Chem. Chem. Phys.*, vol. 16, pp. 11 848–11 863, 2014.

[76] J. M. Olson, "The FMO Protein," *Photosynth. Res.*, vol. 80, pp. 181–187, 2004.

[77] J. F. Imhoff, "Biology of Green Sulfur Bacteria," in *eLS*. Chichester, UK: John Wiley & Sons, Ltd, 2014.

UNIVERSITEIT VAN PRETORIA
UNIVERSITY OF PRETORIA
YUNIBESITHI YA PRETORIA

[78] G. T. Oostergetel, M. Reus, A. Gomez Maqueo Chew *et al.*, "Long-range organization of bacteriochlorophyll in chlorosomes of Chlorobium tepidum investigated by cryo-electron microscopy." *FEBS Lett.*, vol. 581, pp. 5435–5439, 2007.

[79] J. Wen, H. Zhang, M. L. Gross *et al.*, "Native Electrospray Mass Spectrometry Reveals the Nature and Stoichiometry of Pigments in the FMO Photosynthetic Antenna Protein," *Biochemistry*, vol. 50, pp. 3502–3511, 2011.

[80] D. E. Tronrud and J. P. Allen, "Reinterpretation of the electron density at the site of the eighth bacteriochlorophyll in the FMO protein from Pelodictyon phaeum," *Photosynth. Res.*, vol. 112, pp. 71–74, 2012.

[81] M. T. W. Milder, B. Brüggemann, R. van Grondelle *et al.*, "Revisiting the optical properties of the FMO protein," *Photosynth. Res.*, vol. 104, pp. 257–274, 2010.

[82] A. Ishizaki and G. R. Fleming, "Theoretical examination of quantum coherence in a photosynthetic system at physiological temperature." *Proc. Natl. Acad. Sci. U. S. A.*, vol. 106, pp. 17 255–17 260, 2009.

[83] J. Adolphs and T. Renger, "How Proteins Trigger Excitation Energy Transfer in the FMO Complex of Green Sulfur Bacteria," *Biophys. J.*, vol. 91, pp. 2778–2797, 2006.

[84] E. L. Read, G. S. Schlau-Cohen, G. S. Engel *et al.*, "Visualization of Excitonic Structure in the Fenna-Matthews-Olson Photosynthetic Complex by Polarization-Dependent Two-Dimensional Electronic Spectroscopy," *Biophys. J.*, vol. 95, pp. 847–856, 2008.

UNIVERSITEIT VAN PRETORIA
UNIVERSITY OF PRETORIA
YUNIBESITHI YA PRETORIA

[85] A. Camara-Artigas, R. E. Blankenship, and J. P. Allen, "The structure of the FMO protein from Chlorobium tepidum at 2.2 Å resolution," *Photosynth. Res.*, vol. 75, pp. 49–55, 2003.

[86] M. Cho, H. M. Vaswani, T. Brixner *et al.*, "Exciton Analysis in 2D Electronic Spectroscopy," *J. Phys. Chem. B*, vol. 109, pp. 10 542–10 556, 2005.

[87] Y.-C. Cheng and G. R. Fleming, "Dynamics of light harvesting in photosynthesis." *Annu. Rev. Phys. Chem.*, vol. 60, pp. 241–262, 2009.

[88] G. S. Engel, T. R. Calhoun, E. L. Read *et al.*, "Evidence for wavelike energy transfer through quantum coherence in photosynthetic systems." *Nature*, vol. 446, pp. 782–786, 2007.

[89] R. E. Blankenship, J. M. Olson, and M. Miller, "Anoxygenic Photosynthetic Bacteria," pp. 399–435. [Online]. Available: http://www.springerlink.com/index/10.1007/0-306-47954-0

[90] O. I. Keppen, I. A. Berg, N. V. Lebedeva *et al.*, "Chlorobaculum macestae sp. nov., a new green sulfur bacterium," *Microbiology*, vol. 77, pp. 69–77, 2008.

[91] D. E. Tronrud, J. Wen, L. Gay *et al.*, "The structural basis for the difference in absorbance spectra for the FMO antenna protein from various green sulfur bacteria," *Photosynth. Res.*, vol. 100, pp. 79–87, 2009.

[92] N. G. Jerlov, *Marine Optics*, ser. Elsevier Oceanography Series. Elsevier Science, 1976.

[93] G. Hauska, T. Schoedl, H. Remigy *et al.*, "The reaction center of green sulfur bacteria," *Biochim. Biophys. Acta - Bioenerg.*, vol. 1507, pp. 260–277, 2001.

UNIVERSITEIT VAN PRETORIA
UNIVERSITY OF PRETORIA
YUNIBESITHI YA PRETORIA

[94] P. C. Maxwell and J. Biggins, "Role of cyclic electron transport in photosynthesis as measured by the photoinduced turnover of P700 in vivo." *Biochemistry*, vol. 15, pp. 3975–3981, 1976.

[95] W. Lockau and W. Nitschke, "Photosystem I and its bacterial counterparts," *Physiol. Plant.*, vol. 88, pp. 372–381, 1993.

[96] L. Hui, "Biological sciences, Green sulfur bacterium, Chlorosomes, Chlorobium tepidum, Light-harvesting antennae," Ph.D. dissertation, The Pennsylvania State University, 2006.

[97] G. S. Orf, D. M. Niedzwiedzki, and R. E. Blankenship, "Intensity Dependence of the Excited State Lifetimes and Triplet Conversion Yield in the Fenna-Matthews-Olson Antenna Protein," *J. Phys. Chem. B*, pp. 2058–2069, 2014.

[98] S. Santabarbara, G. Agostini, A. P. Casazza *et al.*, "Chlorophyll triplet states associated with Photosystem I and Photosystem II in thylakoids of the green alga Chlamydomonas reinhardtii," *Biochim. Biophys. Acta - Bioenerg.*, vol. 1767, pp. 88–105, 2007.

[99] B. Di Bartolo, "Fluorescence Spectroscopy and Energy Transfer Processes in Biological Systems," in *Biophotonics Spectrosc. Imaging, Sensing, Manip.*, B. Di Bartolo and J. Collins, Eds., ch. 6. Springer Science & Business Media, 2010.

[100] V. I. Novoderezhkin, M. A. Palacios, H. van Amerongen *et al.*, "Excitation Dynamics in the LHCII Complex of Higher Plants: Modeling Based on the 2.72 Å Crystal Structure," *J. Phys. Chem. B*, vol. 109, pp. 10 493–10 504, 2005.

UNIVERSITEIT VAN PRETORIA
UNIVERSITY OF PRETORIA
YUNIBESITHI YA PRETORIA

[101] F. Müh, M. E.-A. Madjet, and T. Renger, "Structure-Based Identification of Energy Sinks in Plant Light-Harvesting Complex II," *J. Phys. Chem. B*, vol. 114, pp. 13 517–13 535, 2010.

[102] F. Müh, M. E.-A. Madjet, and T. Renger, "Structure-based simulation of linear optical spectra of the CP43 core antenna of photosystem II," *Photosynth. Res.*, vol. 111, pp. 87–101, 2012.

[103] C. Kreisbeck and A. Aspuru-Guzik, "Efficiency of energy funneling in the photosystem II supercomplex of higher plants," *Chem. Sci.*, pp. 1–23, 2015.

[104] H. Visser, F. Kleima, I. van Stokkum *et al.*, "Probing the many energy-transfer processes in the photosynthetic light-harvesting complex II at 77 K using energy-selective sub-picosecond transient absorption spectroscopy," *Chem. Phys.*, vol. 210, pp. 297–312, 1996.

[105] F. J. Kleima, C. C. Gradinaru, F. Calkoen *et al.*, "Energy transfer in LHCII monomers at 77K studied by sub-picosecond transient absorption spectroscopy." *Biochemistry*, vol. 36, pp. 15 262–15 268, 1997.

[106] C. C. Gradinaru, S. Özdemir, D. Gülen *et al.*, "The Flow of Excitation Energy in LHCII Monomers: Implications for the Structural Model of the Major Plant Antenna," *Biophys. J.*, vol. 75, pp. 3064–3077, 1998.